An integrated remote sensing-GIS approach for the analysis of an open pit in the Carrara marble district, Italy: Slope stability assessment through kinematic and numerical methods

(Article begins on next page)

02 May 2024

1 An integrated remote sensing-GIS approach for the analysis of an open

2 pit in the Carrara marble district, Italy: slope stability assessment

3 through kinematic and numerical methods

4

5 Authors: Francioni, M. (a); Salvini, R. (b); Stead, D. (a); Giovannini, R. (b); Riccucci, S. (b); Vanneschi,

6 C. (b); Gullì, D. (c).

7

8 (a) Department of Earth Sciences, Simon Fraser University, Burnaby, BC, Canada.

9 (b) Department of Environment, Earth and Physical Sciences and Centre of Geotechnologies, University

10 of Siena, San Giovanni Valdarno, AR, Italy.

11 (c) Regione Toscana - Operative Unit of Mining Engineering (U.O.I.M.) AUSL 1 Carrara,Tuscany, Italy

12

13 Corresponding author: Francioni, M. Department of Earth Sciences, Simon Fraser University, Burnaby,

14 BC, Canada, 8888 University Drive, Burnaby, B.C., Canada, V5A 1S6. E-mail: mfrancio@sfu.ca. Phone:

15 778-782-7288

16

17 **Abstract**

18

19 Over the last decade, terrestrial laser scanning and digital terrestrial photogrammetry techniques have

20 been increasingly used in the geometrical characterization of rock slopes. These techniques provide

21 innovative remote sensing tools which overcome the frequent problem of rock slope inaccessibility.

22 Comprehensive datasets characterizing the structural geological setting and geometry of the slopes can be

23 obtained. The derived information is very useful in rock slope investigations and finds application in a

24 wide variety of geotechnical and mine operations. In this research an integrated remote sensing – GIS

25 approach is proposed for the deterministic kinematic characterization of the Lorano open pit in the Apuan

26 Alps of Italy. Based on the results of geomatic and engineering geological surveys, additional

27 geomechanical analysis using a 3D finite difference method will be presented in order to provide a better

28 understanding of the role of stress-induced damage on slope performance.

29

30 **Keywords**: Unmanned aerial vehicle; terrestrial laser scanning; GIS, deterministic kinematic analysis, 3D

31 finite difference method; stress-induced damage.

32

33

1. Introduction

Surface mining represents a major important economic activity for many countries worldwide. With the high number of people working in the mining industry, safety in the workplace has become an over-riding priority. In this context, the use of new technologies to study and monitor mining and quarrying areas can play a very important role in risk assessment and management.

This paper, developed within the framework of the Italian National Research Project PRIN2009, provides a new approach for the study of open pit quarry slopes based on the integrated use of remote sensing techniques for deterministic stability analyses using combined simple kinematic analysis techniques and three dimensional Finite Difference Method (FDM) stress models. The research describes the case study of the Lorano open pit, characterized by a buttress- shaped remnant from previous excavation activities. The quarry is located in the Carrara district of the Apuan Alps (Italy) which is the most active marble quarrying region in Europe. Here several quarry walls reach hundreds of meters in height and are dominated by natural slopes with very complex morphology. In such an environmental context conventional structural and engineering geological surveys can only be executed at the foot of the slope; therefore, the data obtained from these surveys often provides an incomplete knowledge of the area. An alternative approach would be to have surveys carried out by technicians who are trained in rope access climbing on high rock slopes. There are however limitations and technical difficulties in the implementation of such rope access survey methods, including the close proximity to the quarry wall which compromises visibility and the ability to recognize large-scale geological features, as well as the unavailability of suitable cartographic maps. For these reasons, the use of remote sensing techniques has the potential to significantly increase the information on the geometry and the structural geological setting of quarry slopes.

In this research, two different remote sensing techniques have been used to complement the data obtained from traditional engineering geological surveys. The remote sensing methods used included Terrestrial Laser Scanning (TLS) and Unmanned Aerial Vehicle (UAV) based Digital Terrestrial Photogrammetry (DTP). Several authors have demonstrated the use of TLS and DTP in the study of rock slopes and the advantages that these techniques offer in the structural geological and kinematic analysis of rock slopes [30], [3], [38], [20], [79], [50], [31], [54], [77], [78], [69], [71]. Although UAV technology has been increasingly used in the last few years there remain few published references related to the study of rock slopes [42], [60], [22].

Information gained from these remote sensing techniques was used in this case study for analysing the open pit and overhanging quarry slopes. Two different analyses were carried out; the first, a kinematic analysis to examine the most probable slope failure mechanism and the second a FDM study focused on

68 understanding the stress distribution within the slope. The kinematic analysis was performed using an

69 integrated remote sensing – Geographic Information System (GIS) approach.

70 This allowed for a deterministic kinematic analysis based on the geometry of the slope and joint sets.

71 Based on a similar concept, different approaches were used by Brideau et al. [13] and Salvini and

72 Francioni [70]. Brideau et al. [13] compared the wedge intersection vector orientations with the

73 topographic surfaces from a DSM to understand the influence of three-dimensional topography on slope

74 stability analysis. Salvini and Francioni [70] carried out a form of "kinematic back-analysis" using the

75 joint attitudes to identify the areas on the slope that could be affected by future failures.

76 The FDM analysis was carried out using a simplified 3D model derived from TLS and topographic map

77 at scale of 1:2,000 and focused on characterisation of the rock slope stress distribution. It is known from

78 literature how stress-induced damage due to excavation can be a frequent problem in mining and

79 quarrying and the presence of such stress-induced fractures was observed in the study area in this and

80 previous studies [18], [52] and [17]. These newly generated excavation stress-induced brittle fractures

81 may be an important consideration in the stability of an area and their study could decrease the risk of

82 failure and increase the quality of marble in future extraction works. The principal aim of this study was

83 to understand the stress-induced damage caused by the in-situ stress acting in the area and/or the

84 excavation processes. Several authors have studied the relationship between the acting in-situ stresses, the

85 excavation process and brittle fracturing in excavation areas, particularly in underground mining [14],

86 [15], [28], [29], [16]. In this research the Itasca^{TM} FLAC3D code [49], was used for modelling of

87 excavation induced stress in the quarry slopes.

88

89 **2. The Lorano open pit case study**

90

91 The Lorano open pit is located in the Carrara district where marble quarrying is the most important

92 economic activity. Marble extraction in this area has a long history dating back to the Roman Empire (VI

93 – II B.C). Today the Carrara district is the most important marble mining area in Europe with more than

94 100 active quarries and a production of around 1,000,000 tons/year of blocks and aggregated gravels [18].

95 Geologically, the Apuan Alps belong to the Northern Apennines and are a compressional fold-thrust belt

96 formed during the Oligocene due to the collision between the Corsica-Sardinia microplate and the Italian

97 peninsula [4], [52], [17].

98 Evidence for two main tectonic phases can be found in this area. During the first so-called D1 phase (late

99 Oligocene-very early Miocene), there was compression associated with under-thrusting of the Adriatic

100 plate, and deposition following the North-East direction of the Tuscan Nappe and the Ligurids non-

101 metamorphic units. In these conditions, limestone, dated at 180 My, was metamorphosed to marble.

102   Related to this event, is the formation of the metamorphic foliation (S1) that represents the axial plane of

103   sheath folds (from microscopic to kilometre scale) that characterize the major part of the Apuan Alps. The

104   general S1 direction is relatively constant from N 130° E to N 160° E. This metamorphic foliation

105   represents a direction of weakness in the marble in the Carrara district and, although it is not a true open

106   discontinuity set, it can have an important control on the nucleation and propagation of brittle fracturing

107   [18], [52] and [17]. During the second phase (D2), which started in the early Miocene, compression

108   continued so that all the structures that had developed during D1 were re-folded into complex, antiformal

109   stack geometry with the presence of parasitic folds. Subsequently, compression ended during the last

110   stages of the D2 phase and brittle rather than ductile tectonics occurred. This step was characterised by

111   open and kink folds and normal extension faults with low and high dips. This extensional phase caused

112   stretching, denudation and uplift phenomena, bringing higher and lower structures to the same level. In

113   this context, the Apuan Alps now represent a wide tectonic window within the thickened Apennine Nappe

114   [17].

115   The Lorano open pit is located in the normal limb of the "Pianza Anticline", between the "Carrara

116   syncline" in the South-West, and the "Vallini syncline" in the North-East. The open pit is characterized

117   by a rock buttress shape, a remnant of previous excavation activities left to ensure the stability of the rock

118   slope to the rear. The marble buttress is accessible from three sides and is approximately 150 m high and

119   between 30 to 50 m wide (Figure 1). In the study area there are two different types of marble outcrops:

120   the "Ordinario marble", that characterizes the buttress, and the "Venato marble" a natural outcrop

121   occurring on the mountain slope above.

Figure 1. Perspective view of the study area: Lorano open pit walls characterized by the rock buttress shape (the scale is indicative only); inset map shows the location of the study area.

3. Geomatic and engineering geological surveys

Most of the open pit walls in the study area are hundreds of meters high and are dominated by natural slopes with very complex morphology which can be a source of danger for workers below. In such an environment, engineering geological surveys are traditionally executed only in accessible areas at the foot of the slope. The data obtained from these surveys fails to provide complete information of the entire slope as required for deterministic slope analysis.

Quarry wall inspections are conducted once a year by rope access climbers but are often constrained by technical difficulties, low visibility compromising the recognition of large-scale geological features, and high cost. Remote sensing techniques can provide an excellent alternative and TLS and DTP in particular are being increasingly used in the study of such areas. Using these techniques it is possible to obtain very detailed information on the structural geological setting and slope geometry, even in the case of inaccessible steep slopes. The integrated use of DTP and TLS for the study of the buttress and the

139 overhanging slope will be shown in this paper. Special emphasis will be given to the use of UAV for the

140 DTP survey.

141

142 *3.1 Unmanned Aerial Vehicle for photogrammetric surveys*

143

144 Digital terrestrial photogrammetry is a remote sensing technique in which the geometric properties of

145 objects are determined by the measurement of photographic images. DTP is used in many different fields,

146 including topographic mapping, architecture, engineering, and, more recently, engineering geology [67],

147 [44], [76], [33], [34]. Slama [73], Linder [56], and Kraus [53] provide further details on the theory of this

148 technique.

149 Given that pseudo-perpendicular directions of acquisition are necessary owing to the height and steepness

150 of the slopes; traditional remote sensing techniques such as aerial photogrammetry are generally not

151 suitable. The authors have previously discussed the advantages and disadvantages of using different

152 methodologies for photogrammetric data acquisition depending on the slope morphology and the

153 accessibility of rock faces [77], [78], [33], [34]. In this case, considering the elevation and the complex

154 geometry of the buttress (Figure 1), an UAV was used to acquire high spatial resolution images. The

155 survey was carried out by mounting a stabilized digital camera Sony NEX-5N onto a Falcon 8 (Asctec

156 Gmbh) vehicle (Figure 2A and B). The physical CCD frame size of the cameras is 23.5 x 15.6 mm, while

157 the resolution is 16.1 Megapixels.

158 Based on a flight plan, photographs were automatically taken in order to cover the whole site acquiring

159 vertical strips of images with a minimum 70% overlap and 30% sidelap. Auto-positioning of the UAV

160 was controlled by the integrated inertial measurement unit. Due to the complex morphology of the area

161 and the buttress shape, three different lines-of-sight were used during the photogrammetric survey. Figure

162 2C shows the orthophoto of the whole open pit and highlights the three different lines-of-sight.
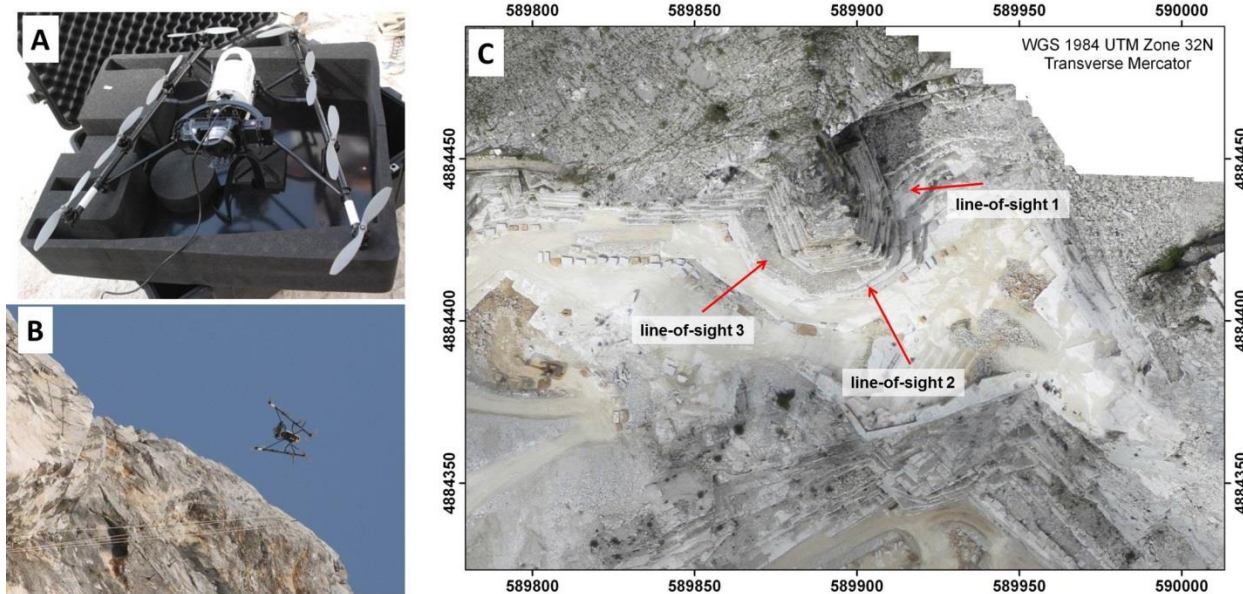
163

164

165 Figure 2. UAV survey: the Falcon 8 with stabilized digital camera Sony NEX-5N (A), vehicle during the

166 flight on the right (B) and orthophoto of the open pit with the three different lines-of-sight used during the

167 photogrammetric survey (C).

168

169 Based on the sensor format, horizontal and vertical fields of view varied with the distance from the walls;

170 Table 1 shows the image size of the utilized camera.

	Image size (pixel)	Image size (mm)
Width	3935	333.2
Height	2620	221.8

171 Table 1. Photogrammetric image size (300 dpi).

172

173 With the objective of obtaining very precise output, 91 natural Ground Control Points (GCP) were

174 measured on the buttress walls using a Leica[TM] TCRP 1203+R1000 reflectorless Total Station. The GCPs

175 are points with known coordinates that must be recognizable on the photographs to facilitate their exterior

176 orientation process (procedure used to define the camera position, rotation and its line-of-sight at the

177 instant of the exposure [73], [56], [53]) that was executed by means of the Leica Photogrammetric Suite

178 (LPS) module of the ERDAS[TM] IMAGINE software. The Root Mean Square Error (RMSE) in image and

179 ground units (respectively pixel and cm) obtained for each strip during the absolute orientation process is

180 shown in Table 2.

181

182

183

Line-of-sight (degrees to North)	RMSE (image unit, pixel)	RMSE (ground unit, mm)
1 (270)	2.3	33
2 (330)	4.7	48
3 (50)	2.7	35

184   Table 2. Line-of-sight, image and ground RMSE.

185

186   *3.2 Terrestrial laser scanning*

187

188   In addition to DTP, terrestrial laser scanning was used to provide additional geometric information about

189   the buttress and to validate the data obtained from the photogrammetric survey. TLS is a survey technique

190   for rapidly obtaining the geometry of objects with high precision. Several types of laser scanner currently

191   exist with different measurement principles and technical specifications [7], [37]. In this paper, a Riegl^{TM}

192   Z420i laser scanner was used for the survey. This instrument uses time-of-flight technology to determine

193   distances to an object at a maximum distance of about 1 km.

194   Considering the geometry of the buttress, three point clouds were acquired to limit the occlusions in the

195   output data; the slope scanning resolution was set to 0.07 m at a distance of 300 m. Sturzenegger and

196   Stead [78] and Francioni et al. [34] discussed the complexity of aligning several point clouds in the same

197   reference system through the registration process. The integrated use of Total Station (TS), differential

198   GPS (Global Positioning System) can be adopted to overcome problems related to the registration

199   process. In this case study 15 High-Definition Surveying (HDS) targets were used in the TLS data

200   acquisition whose absolute coordinates were acquired by a TS topographic survey. The targets were

201   automatically recognized by the Leica^{TM} Cyclone software (used also in the TLS data post-processing) so

202   that the registration could be easily computed by assigning them absolute coordinates. The topographic

203   survey played an important role in the registration process and will be described in more detail in the

204   following section.

205

206   *3.3 Topographic survey*

207

208   The topographic survey was carried out by means of the Leica^{TM} TCRP 1203+R1000 reflectorless Total

209   Station and two geodetic Leica™ 1200 GPS receivers. They were essential for the acquisition of the HDS

210   targets and GCPs for photogrammetry. During the TS survey, the intersection method was used to relate

211   all the measurements to a unique reference system. Using this technique it was possible to locate the TS

212   in different positions (suitable for the acquisition of HDS targets and GCPs) and to relate all the

213   measurements to the first station (called "Master Station"). The use of the TS and the intersection

214   methods are explained in detail in Francioni et al. [36] and Francioni et al. [34].

215 The GPS survey was used to determine the absolute coordinates of all the points measured with the TS; to

216 accomplish this, a GPS receiver was set up in the same position as the Master Station and the absolute

217 coordinate of the latter determined. Subsequently, a second GPS receiver was utilized to obtain the zero-

218 Azimuth for the TS and, finally, the absolute coordinates of all the measured points determined. The

219 differential GPS surveys were performed in static modality with an acquisition time of up to 3 hours. The

220 coordinates of the points acquired with this technique were corrected by post-processing procedures using

221 contemporary data recorded by two permanent GPS stations (*Lucca* and *Borgo a Mozzano*). The

222 orthometric heights of the Master and the zero-Azimuth stations were also calculated in collaboration

223 with the Italian Military Geographical Institute.

224

225 *3.4 Engineering geological survey*

226

227 In order to provide more information about the structural geological setting of the slope and the

228 characteristics of the rock mass and joint surfaces, an engineering geological survey was carried out. Due

229 to the inaccessibility of the area, it was possible to carry out the scan lines only at the toe of the slope

230 (Figure 3). Seven scan lines were performed and more than 100 surfaces measured. Of these, only 77

231 were then used for the definition of the main joint sets. The remain surfaces were identified as brittle

232 fractures and, due to their different origin, irregular shape and unreliability in their measurement, they

233 were not considered in the definition of the main joint sets. Data from scan lines was used for the

234 characterization of rock mass according to the Bieniawski Rock Mass Rating (RMR, 1989) method. The

235 RMR system is a rock mass quality classification developed by the South African Council for Scientific

236 and Industrial Research [8] and subsequently updated in 1989 [78]. The Geological Strength Index (GSI)

237 was also estimated based on the rock mass structure and the rock discontinuity surface condition. This

238 method, used widely by the scientific community after its introduction [45], is not intended as a rock mass

239 classification, but rather to reflect the rock mass quality. The GSI value was then applied to estimate the

240 rock mass parameters in the Hoek-Brown strength criterion. The application and limitations of the GSI for

241 underground openings and rock slopes were recently reviewed by Marinos et al. [57] and Hoek and
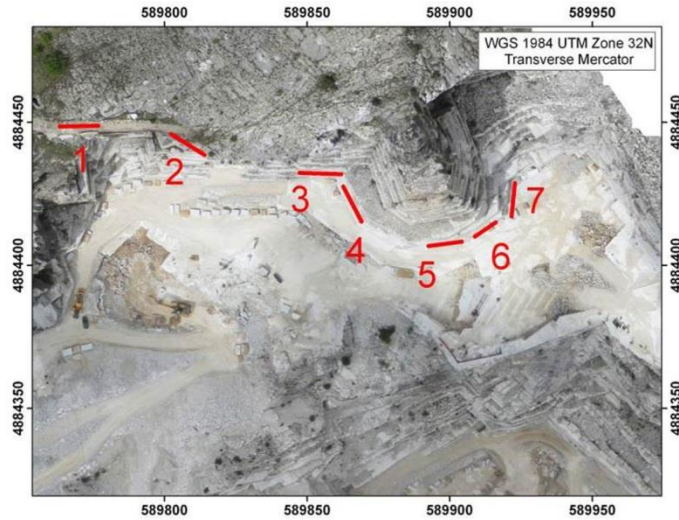
242 Diederichs [47].

243

Figure 3. Orthophoto of the open pit with scan lines

4 Data processing and deliverables

In this case study the UAV system, by limiting blind spots, played a very important role in the acquisition of the photographs of the whole study area. The exterior orientation of the photographs was obtained through the use of the 91 GCPs measured by the topographic survey. After the exterior orientation process, a stereographic model of the buttress was built and used for the stereo-interpretation of structural geological features including joint attitude, spacing and trace length. These features were stereo-restituted using the Stereo Analyst module of ERDAS^{TM} IMAGINE; the joint attitude was represented in the stereoscopic model by triangles drawn co-planar with the discontinuities, while the spacing and trace length were shown using 3D lines. Figure 4A shows stereographic representation of the discontinuities measured on the slope using DTP. The three TLS point clouds acquired during the survey were registered using the HDS targets and allowed the construction of a unique 3D model of the buttress. As mentioned above, using the topographic surveys and the intersection method it was possible to align GCPs and HDS targets in the same reference system with an estimated error of approximately 5 mm. In this way, the stereoscopic model from DTP and the TLS 3D model were integrated and used for the construction of a detailed full 3D model with high resolution orthophotos of the buttress (Figure 5).

The DTP approach provides a high level of data interpretability during the stereo-restitution but can be prone to human error. For this reason, the attitude of the discontinuity surfaces and slopes was also extracted from the TLS point clouds using the Leica^{TM} Cyclone software through a semi-automatic procedure. In practice, several points (at least three) representing the surface under investigation must be selected on the point cloud; the software automatically recreates the surface and determines the attitude of

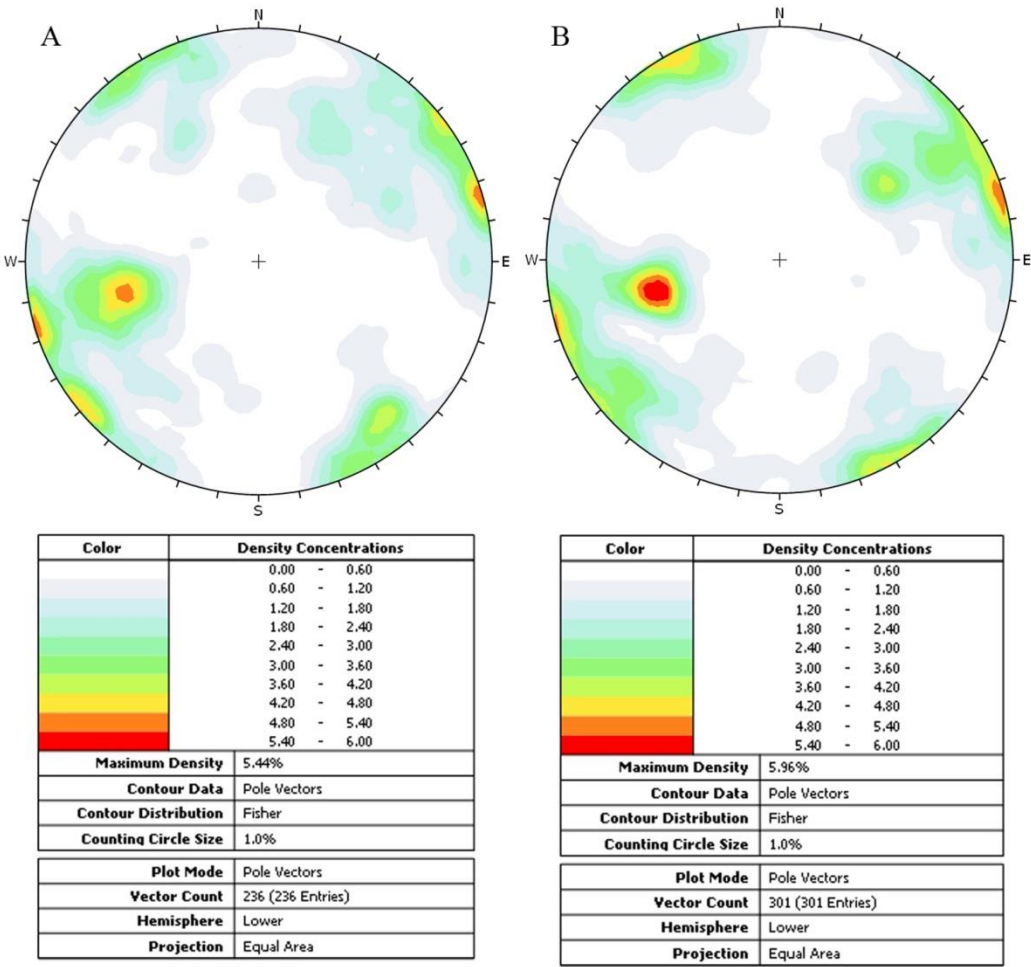268   its pole. Figure 4B shows the stereographic representation of the discontinuities measured on the slope
269   using TLS.

Color	Density Concentrations	
	0.00	0.60
	0.60	1.20
	1.20	1.80
	1.80	2.40
	2.40	3.00
	3.00	3.60
	3.60	4.20
	4.20	4.80
	4.80	5.40
	5.40	6.00
Maximum Density	5.44%	
Contour Data	Pole Vectors	
Contour Distribution	Fisher	
Counting Circle Size	1.0%	
Plot Mode	Pole Vectors	
Vector Count	236 (236 Entries)	
Hemisphere	Lower	
Projection	Equal Area	

Color	Density Concentrations	
	0.00	0.60
	0.60	1.20
	1.20	1.80
	1.80	2.40
	2.40	3.00
	3.00	3.60
	3.60	4.20
	4.20	4.80
	4.80	5.40
	5.40	6.00
Maximum Density	5.96%	
Contour Data	Pole Vectors	
Contour Distribution	Fisher	
Counting Circle Size	1.0%	
Plot Mode	Pole Vectors	
Vector Count	301 (301 Entries)	
Hemisphere	Lower	
Projection	Equal Area	

270

271   Figure 4. Stereographic representation of measurements obtained from DTP (A) and TLS (B).
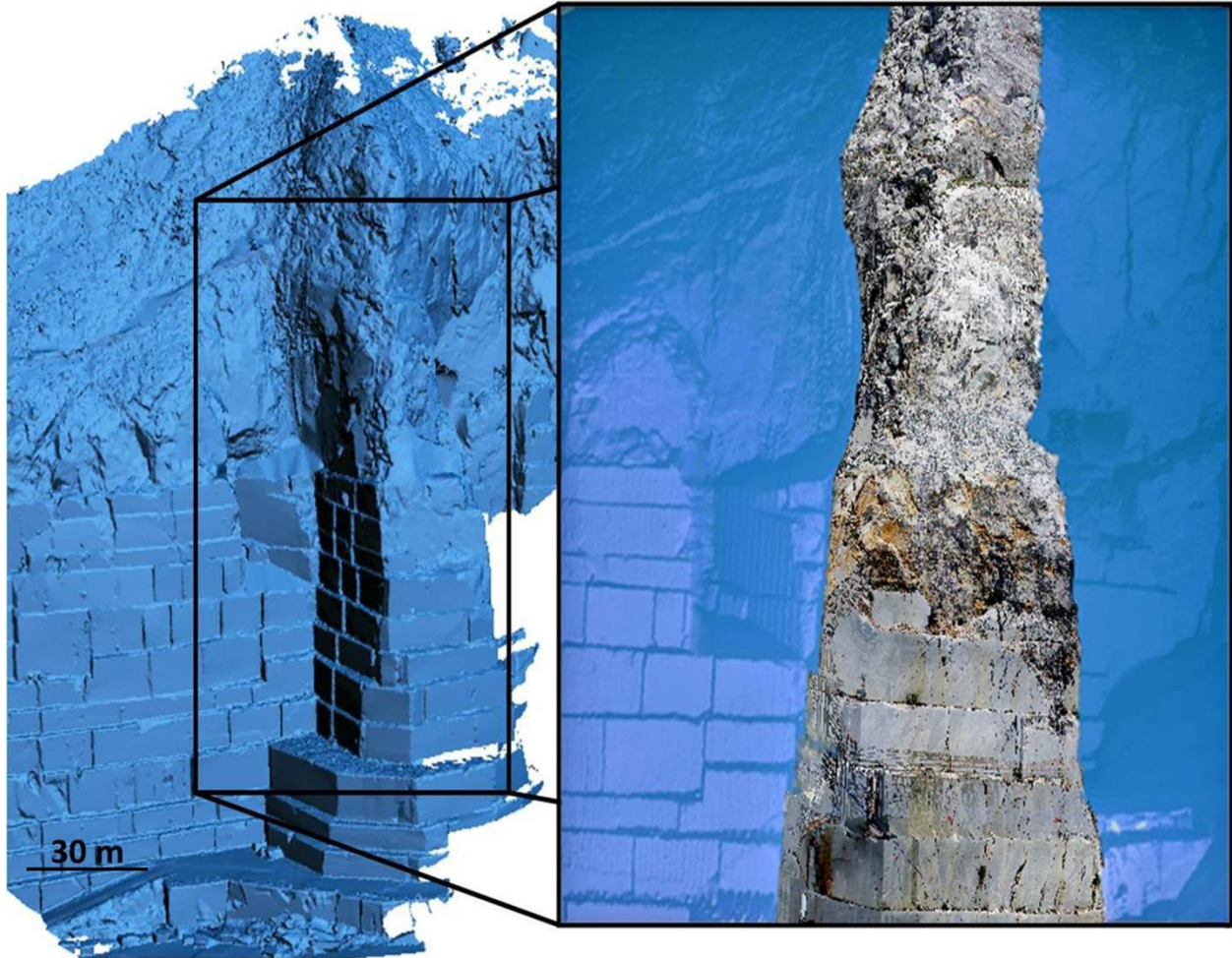
272

273

274   Figure 5. Integration of TLS and UAV photogrammetric data in the construction of the 3D model with

275   aligned orthophotos of the buttress.

276

277   All the measurements obtained from TLS and DTP were then integrated in a final stereographic

278   representation and the joint sets determined (Figure 6 and Table 3). K1, K2 and K3 represent the three

279   main joint systems surveyed with these techniques and S1 represent the structures associated with the

280   metamorphic foliation S1 which characterizes the Apuan Alps (see section 2). Table 3 also shows the

281   measurements of spacing and trace length carried out using the remote sensing data. However, due to the

282   difficulty in defining the trace length in the photogrammetric model (especially when the joint spacing is

283   small as often is the case in the Carrara marble district) and to fact that these parameters were required

284   in the following analyses, these measurements should be considered as a preliminary approximate
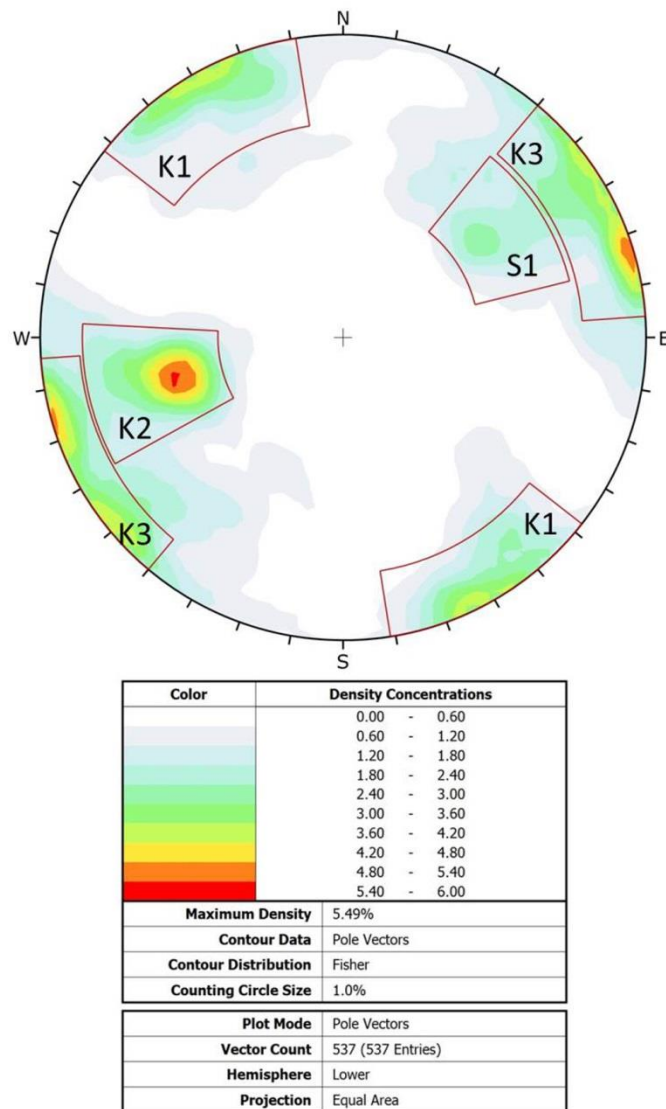
285   estimation only.

286

287

Color	Density Concentrations
	0.00 - 0.60
	0.60 - 1.20
	1.20 - 1.80
	1.80 - 2.40
	2.40 - 3.00
	3.00 - 3.60
	3.60 - 4.20
	4.20 - 4.80
	4.80 - 5.40
	5.40 - 6.00
Maximum Density	5.49%
Contour Data	Pole Vectors
Contour Distribution	Fisher
Counting Circle Size	1.0%
Plot Mode	Pole Vectors
Vector Count	537 (537 Entries)
Hemisphere	Lower
Projection	Equal Area

288

289   Figure 6. Integration of measurements obtained from TLS and DTP.

290

Joint set	Dip (deg)	Dip Direction (deg)	Trace length (m)	Spacing (m)
K1	88	150	10 to 30	1 to 3
K2	54	077	10 to 30	1 to 3
K3	87	243	10 to 30	1 to 3
S1	52	235	2 to 20	1 to 10

291   Table 3. Data obtained from DTP and TLS.

292

293   Conventional engineering geological survey was necessary to assess the accuracy of the joint sets present

294   at the toe of the slope and to physically and mechanically characterise the discontinuities according to the

295   RMR method. Data obtained from this survey is provided in Figure 7 and Table 4; the results gained from

296   the rock mass rating show a good quality rock mass with an RMR value equal to 76. However, Figure 7

297   and Table 4 also show that the joint set distribution at the toe of the slope was slightly different to that

298   determined from DTP and TLS. Therefore, data in Table 4 may not be fully representative of all the joint

299   sets illustrated in Table 3 since they refer to different locations within the study area. In fact, GSI values

300   also vary within engineered areas (i.e. open pit) compared to the natural rock outcrops (i.e. the above

301   slope). For this reason and considering in detail the characteristics of the marble the GSI was estimated to

302   vary between 50 and 60 in the natural slope and between 70 and 80 in the open pit face. This is probably

303   due to the degree of weathering of the natural slope surface and to the fact that the joint spacing usually
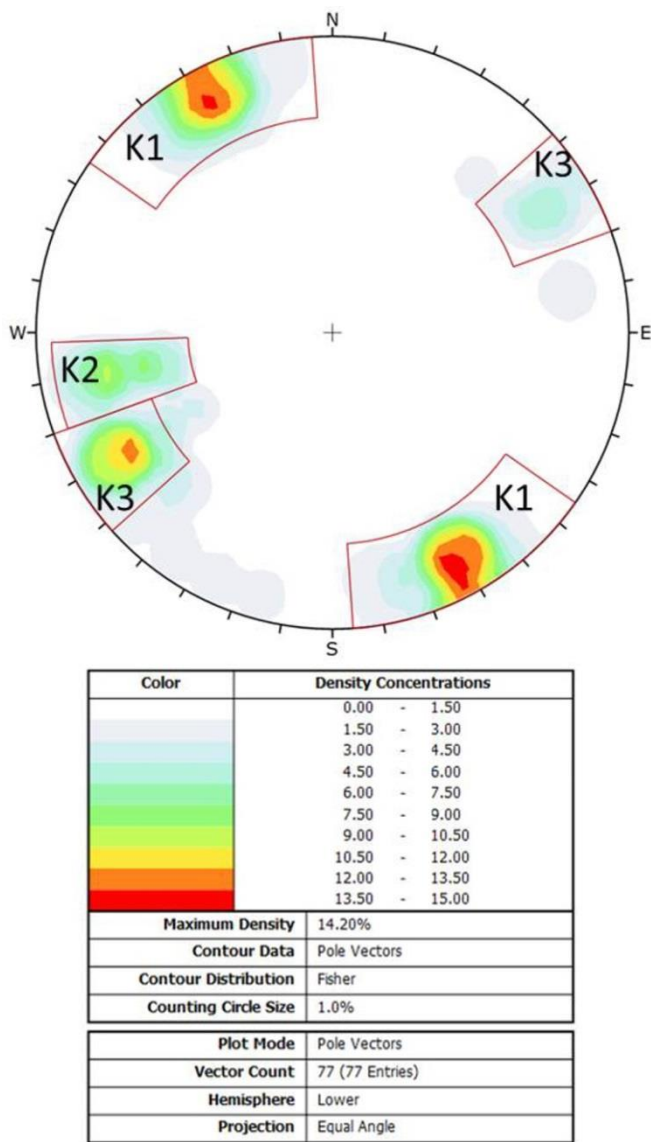
304   increases with depth.

Color	Density Concentrations	
	0.00	-	1.50
	1.50	-	3.00
	3.00	-	4.50
	4.50	-	6.00
	6.00	-	7.50
	7.50	-	9.00
	9.00	-	10.50
	10.50	-	12.00
	12.00	-	13.50
	13.50	-	15.00
Maximum Density	14.20%
Contour Data	Pole Vectors
Contour Distribution	Fisher
Counting Circle Size	1.0%

Plot Mode	Pole Vectors
Vector Count	77 (77 Entries)
Hemisphere	Lower
Projection	Equal Angle

305

306   Figure 7. Stereographic representation of measurements determined from the conventional engineering

307   geological survey.

308

Joint set	K1	K2	K3
Dip/Dip Dir	90°/332°	71°/080°	84°/059°
Spacing (m)	1	1	1.5
Trace length (m)	10 to 20	10 to 20	10 to 20
Aperture (mm)	14	9	11
Infill	Absent	Absent	Absent
Weathering	Slight	Slight	Slight
JRC	4	9	5
JCS (MPa)	98	78	83
Water	Medium inflow	Absent	Medium inflow

309   Table 4. Data obtained from the conventional engineering geological survey (mean values).

310

311   During both the remote sensing and engineering geological surveys, brittle (stress-induced) fractures were

312   identified (Figure 8). It is possible to differentiate these structures from pre-existing discontinuities based

313   on their irregular shape and the lower trace length. These characteristics can make their mapping

314   sometimes challenging with a higher degree of uncertainty and, for this reason the measurements related

315   to the stress-induced fractures were kept separate from those associated with joint sets.
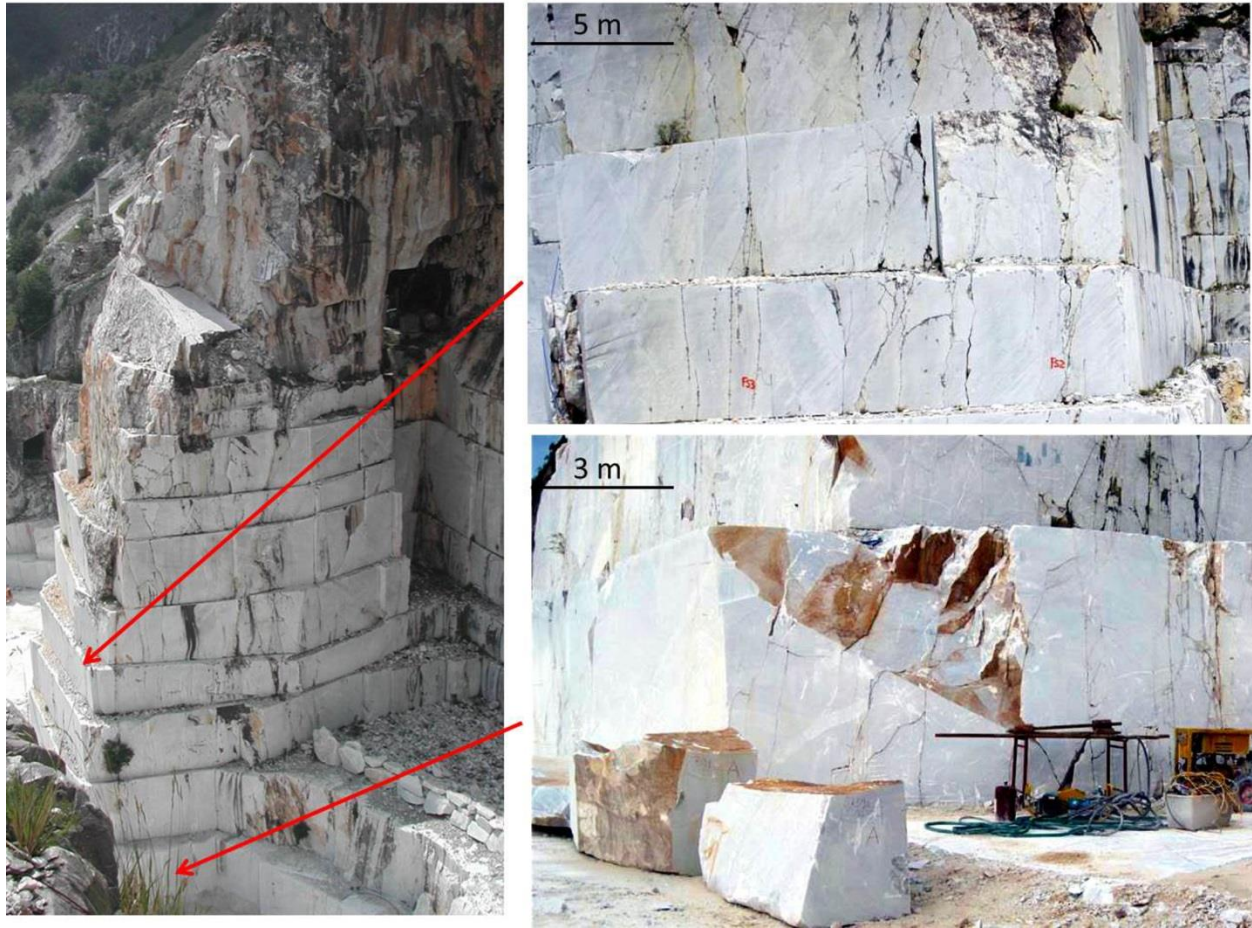
Figure 8. Stress-induced damage noted in the marble buttress during the engineering geological and photogrammetric surveys.

5 GIS and kinematic stability analyses

The kinematic slope stability analysis examines the potential for rock slope failures such as planar, wedge, and toppling due to the presence of unfavourably oriented discontinuities. The analysis considers the relative attitude of the discontinuities and the slope plus the effective friction angle along the joint surfaces. Stereographic projections for the kinematic analysis of these simple failure modes are described in Richards et al. [64] and Hoek and Bray [46]. Various widths of toppling envelope have been proposed by Goodman and Bray [40], Cruden [21], Goodman [39], and Maurenbrecher and Hack [58]. The results of this analysis are strongly influenced by the topography, as already documented by Brideau et al. [13] who proposed the use of software such as Matterocking [50], which compares the wedge intersection vector orientations with the topographic surfaces.

331 In this research, an integrated remote sensing – GIS analysis approach was proposed to overcome the

332 problem of complex geometry. GIS techniques have been used by several authors for slope stability

333 analysis [82], [81], [84], [85], [23], [6], since they provide various functions for capturing, inputting,

334 manipulating, transferring, visualizing, combining, querying, analysing, modelling, and outputting of the

335 geospatial data. The advent of new survey techniques (such as those used in this research) makes this

336 technique even more attractive because they allow a wider range of data to be analysed. In this research

337 the 3D model and the topographic map at scale of 1:2,000, gained from the TLS, were used in the

338 construction of a simplified Digital Surface Model (DSM) of the pit slope.

339 Starting from the DSM, a GIS spatial analysis was performed to highlight the dip direction of the slope

340 faces (Figure 9A). Different colours in Figure 10A represent slopes characterized by varying dip

341 direction. Based on the orientation of the slope faces and using the geo-structural data derived from the

342 geomatic and engineering geological surveys, it was possible to perform a kinematic GIS analysis of

343 slope stability. For each slope face, the steepest safe angle was calculated using the stereographic

344 projection of Dips 6.0 software [66]. The knowledge of the steepest safe angle is very useful for

345 understanding the maximum angle that a slope can be quarried at before subject to potential failures due

346 to interaction with discontinuities. This information was integrated with the steepness of the slope in

347 order to ascertain which areas may be affected by failure. Consequently, a further GIS spatial analysis

348 was carried out and the slope steepness calculated (Figure 9B). In this way, all the necessary information

349 was available to understand where failure mechanisms could occur. A supplementary spatial analysis was

350 carried out to combine the steepest safe angle with the slope steepness in order to further refine the

351 results. The friction angle was assumed to be 32° (with $5°$ of standard deviation) for all the joint systems

352 based on the published literature, [19], [62], [63], [32]. Figure 11 shows the results highlighting the

353 stereographic representation of main joint sets used for the analysis (Figure 10A) and the areas that could

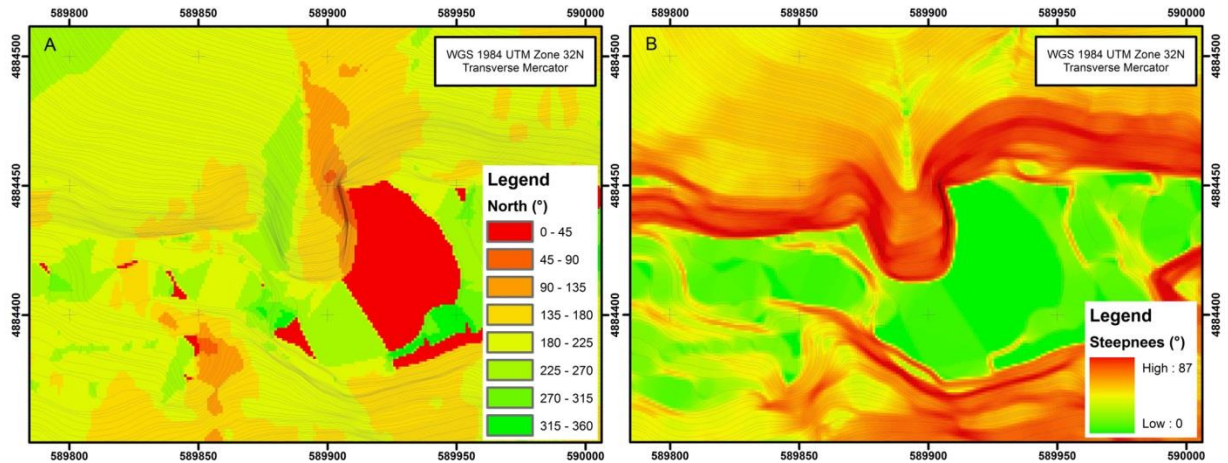354 be affected by planar (Figure 10B), wedge (Figure 10C), and direct toppling failures (Figure 10D).

355

356

357 Figure 9. Dip direction of slope faces (A) and slope steepness (B) calculated with GIS spatial analysis.
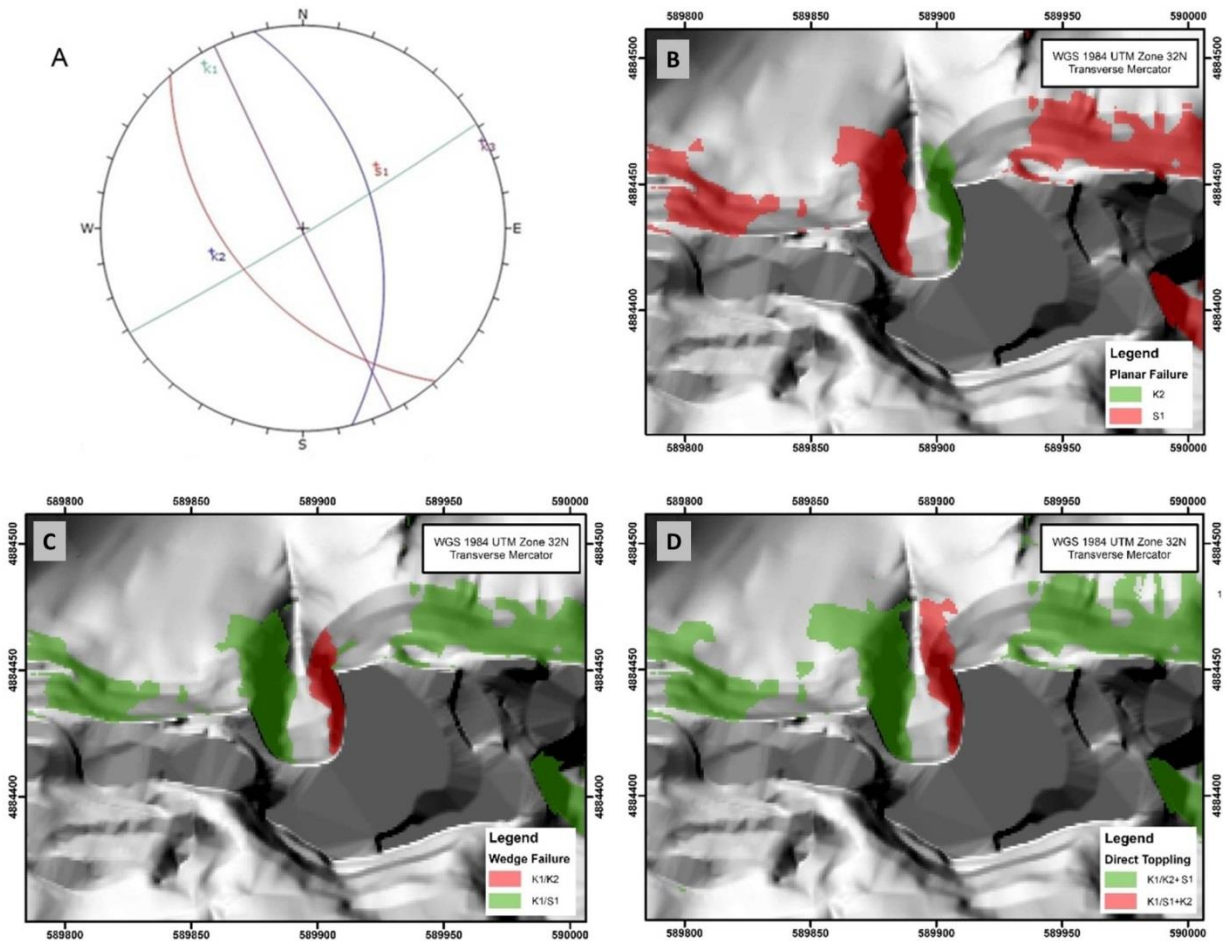
358

359

360 Figure 10. Results of the deterministic kinematic stability analysis: Stereographic representation of joint

361 sets shown in Table 3 (A); areas potentially affected by planar failure (B); areas potentially affected by

362 wedge failure (C); areas potentially affected by direct toppling (D).

363   Maps shown in Figures 10B and 10C highlight a strong similarity due to an important assumption in

364   Rocscience^{TM} [66] software regarding "pure" planar sliding on a single plane; in fact, in these types of

365   analyses, the occurrence of release planes, such as lateral joints, or tension cracks is assumed to allow

366   planar sliding. These planes are not explicitly involved in the conventional kinematic analysis for planar

367   sliding, but it is important to be aware that a release mechanism must normally exist to allow removal of a

368   block from the slope. This means that planar sliding can be considered as a special case of wedge failure

369   where sliding takes place on only one plane, and other planes act as release planes. It should be noted that

370   the foliation S1 was included in the analysis even if it is not a true open discontinuity set. This was

371   undertaken to reflect the fact that the S1 foliation represents a direction of weakness in the rock mass

372   which can have an important control on the dilation, nucleation and propagation of brittle fractures [18],

373   [52] and [17]. This phenomenon is visible in the upper right of Figure 8 where low angle fractures (with

374   irregular shape and direction similar to S1) seem to connect the high angle discontinuities that

375   characterize the buttress face. For this reason, the authorities decided to leave in place wider benches at

376   the base of the buttress with the aim to increase the overall stability and avoid the propagation of new

377   generated fractures between system discontinuities.

378

379   **6 Three dimensional stress analyses using the finite difference method, FLAC3D**

380

381   DTP, TLS and the engineering geological surveys provide fundamental data for an improved

382   understanding of the structural geological setting of the area. Using these methods it was possible to

383   analyse whether the fractures on the slope were related to the complex geological history of the area

384   and/or to the recent excavation activity. In fact, the progress of the excavation can cause the formation of

385   new brittle fractures due to the unloading stress. Their existence in the Carrara marble district (called

386   "*forzature*" by the local technicians) has been the cause not only of damage within the extracted blocks

387   and slabs, but also of several rock fall events as documented by several authors; see e.g. [17] and [18].

388   In this research, the FLAC3D code [49] was used to analyse the stress distribution of the slope using the

389   Finite Difference Method. Although FLAC is a continuum numerical modelling approach and is not

390   appropriate to model a large number of fractures, selected discontinuities with simple intersections can be

391   discretely included as interfaces [55]. Numerous authors have described the use of FLAC for the analysis

392   of rock slopes and open pits [11], [43], [68].

393

394   *6.1 Stress distribution using the induced lithostatic stress*

395   In this study, Rhinoceros^{TM} SR4 software [59] was used with the aim of creating a 3D model closely

396   approximating the true geometry of the slope. TLS point clouds were processed to build the 3D model

397 and then exported into Kubrix software [49] to prepare for simulation using FLAC 3D [49]. Figure 11A-

398 D shows the 3D model created by Rhinoceros[TM] SR4 and Kubrix. Figure 11A shows the initial geometry

399 used to calculate the initial stress distribution. Figure 11B shows the reconstruction of the topography

400 before the marble excavation. Figure 11C and D show the geometry of the buttress and the "history

401 points" (points of interest) respectively; the latter were located at different elevations on the marble

402 buttress and interrogated during the excavation progress.

403

404
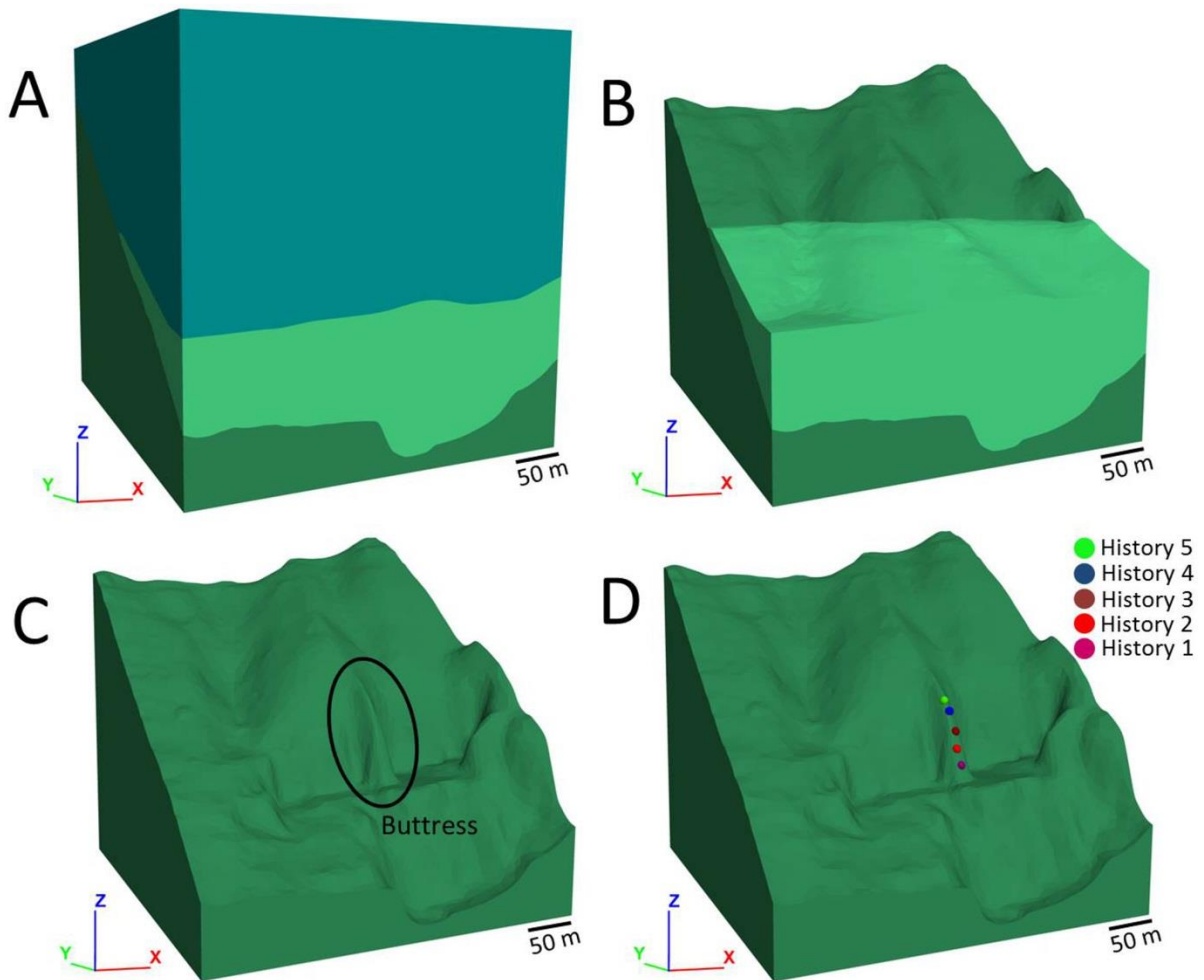
405 Figure 11. 3D model of the marble quarry and buttress created in Rhinoceros[TM] SR4 and Kubrix: Initial

406 model (A), topography pre (B) and post (C) excavation and history points located in the buttress (D).

407

408 The marble was modelled as an elastic material with a unit weight of 27 KN/m^3 with joints not considered

409 at this stage. The isotropic elastic and material option, in FLAC3D, provides the simplest representation

410   of material behaviour and is valid for homogeneous, isotropic, and continuous material that exhibits linear

411   stress-strain behaviour.

412   This decision was made after a careful examination of the literature and that, given the strength of the

413   marble rock mass and the limited depth of the quarry, little yield should occur under compressive stresses.

414   Moreover, this decision was also taken in agreement with the studies carried out by Wiles [83]. Wiles,

415   after a long discussion on the use and reliability of simple versus complex constitutive criteria noted that

416   the use of an elasto-plastic model makes the calibration of the model extremely difficult due the

417   uncertainty of the additional parameters required, (E, V and density vs E,v. Density, intact cohesion,

418   intact friction, dilation, rock mass cohesion, rock mass friction). In essence at this stage in our models we

419   have focused on location of stress concentrations, not yielding of these stresses. The latter would have

420   necessitated the assumptions inherent in scale-dependent downgrading of the rock properties and hence

421   possibly obscured the results. Wiles suggests, for making stress predictions, the use of an accurate

422   geometry and simple model (Homogeneous, elastic modelling is the best option since the only significant

423   parameter that must be specified is the far-field stress state). Table 5 shows the rock properties used in

424   this first simulation (called "Analysis 1").

425

Parameters - Analysis 1	Value
Unit weight (KN/m^3)	27
Deformation modulus (GPa)	48
Poisson's ratio	0.27
Shear modulus (GPa)	19
Bulk modulus (GPa)	34

426   Table 5. Rock material parameters used in Analysis 1

427

428   Since the elevation of the model was approximately 440 meters, the lithostatic vertical stress σ_z (or σ_v)

429   was estimated to be almost 12 MPa at the base of the model. This value was gradually decreased from the

430   bottom to the top so that to be zero at the surface of the initial model. The K values, K_x and K_y in this

431   preliminary analysis were assumed to be equal to 0.4 (Equations 1 and 2).

432

433    $K_x = \sigma_x / \sigma_z$ Equation 1

434    $K_y = \sigma_y / \sigma_z$ Equation 2

435

436   The deformation modulus was calculated using the GSI value and RocData 4.0 software (Rocscience[TM]

437   2014 and Hoek & Diederichs, 2006), while the Shear and Bulk moduli were calculated from equations 3

438   and 4:

439

440 G = E/2(1+ν)   Equation 3

441 K = E/3(1-2ν)   Equation 4

442

443 where G is Shear modulus, K the Bulk modulus and ν the Poisson's ratio.

444

445 The FLAC 3D code allowed the analysis of the stress distribution in the X, Y, and Z directions. Figure 12

446 shows the simulated stress distributions obtained in Analysis 1 in the X (Figure 12B), Y (Figure 12C),
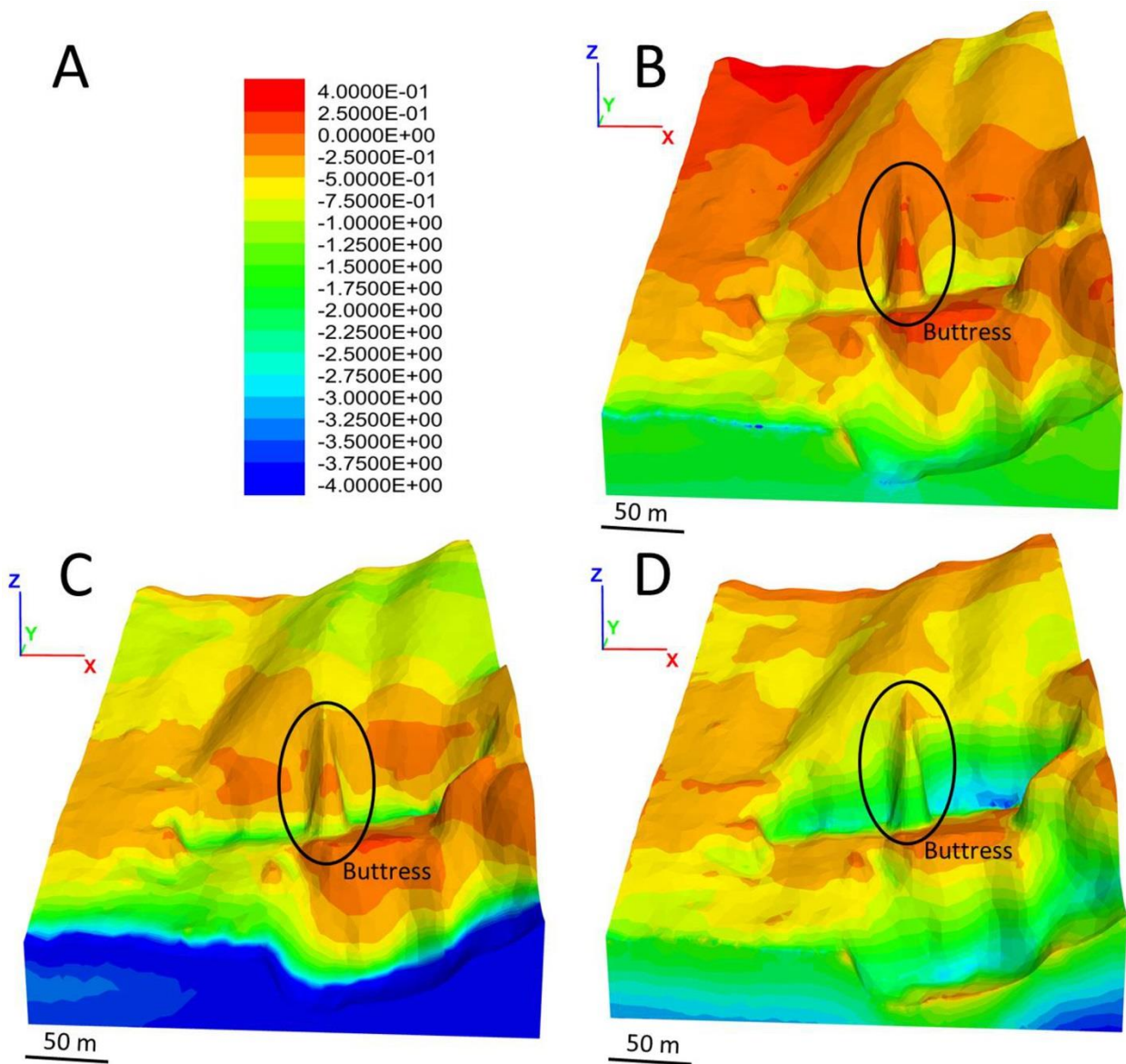
447 and Z (Figure 12D) directions respectively.

448

449

450   Figure 12. FLAC3D models for Analysis 1 showing the simulated stress distribution and magnitude;

451   legend showing stress magnitude in MPa (A), stress distribution in XX direction (B), YY direction (C),

452   and ZZ direction (D).

453

454   The stress values change from negative to positive indicating compressive and tensile stresses

455   respectively. When positive values are present, the stress conditions are in tension and consequently, new

456   fractures may be created, due to the unloading stress. Figure 12 shows positive tensile stress in the

457   buttress with values in the X direction greater than in the Y direction. Figure 13 illustrates the stress state

458   in the X and Y directions as measured at the history points (the x-axis represents the number of

459   calculation steps in the analysis and the y-axis the value of stress in MPa).
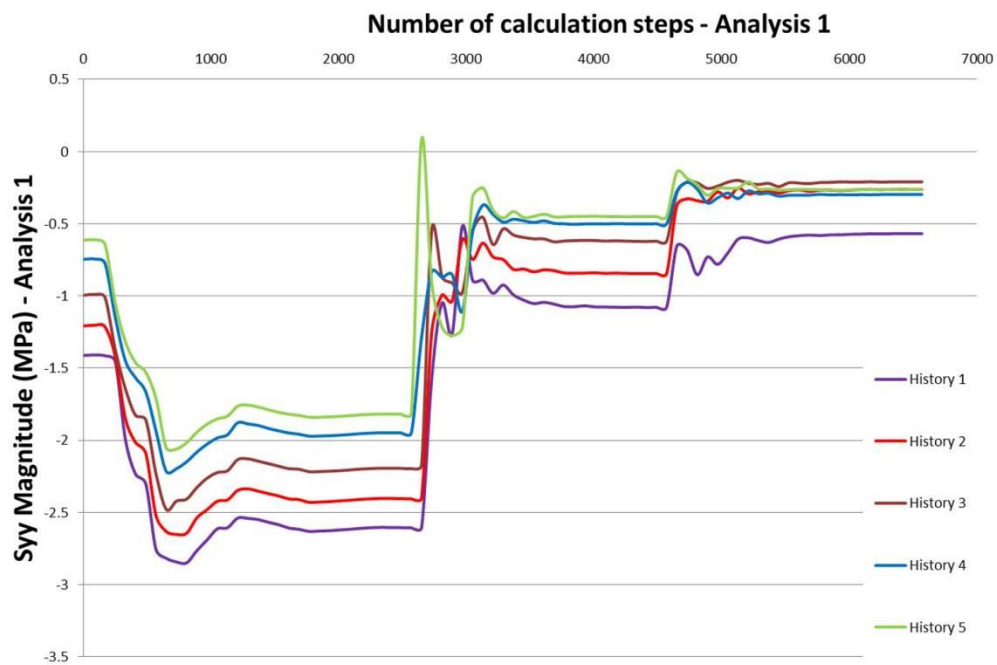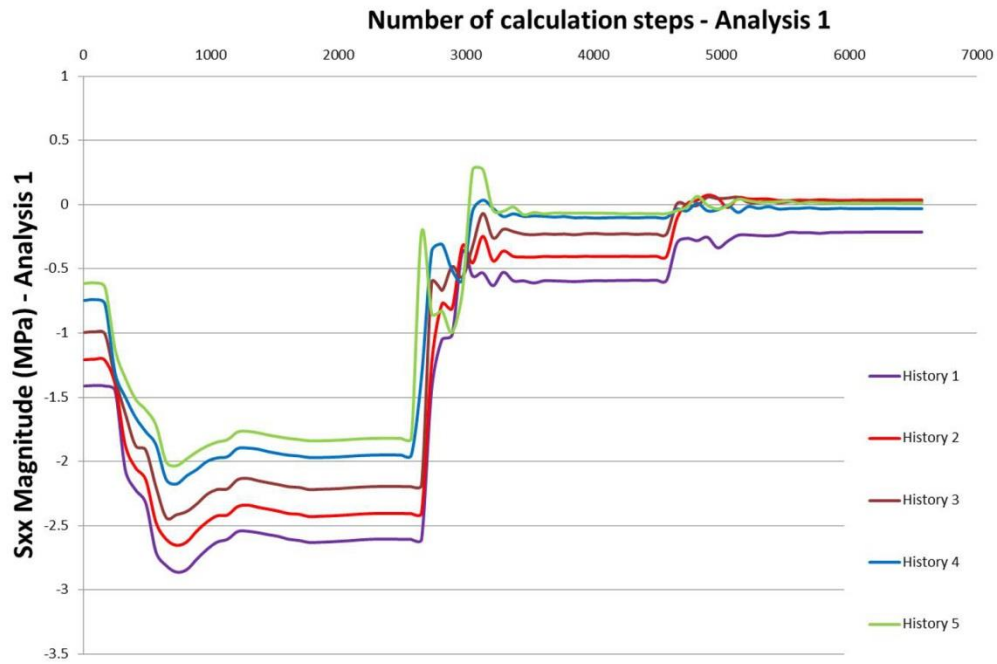
460

461 Figure 13. Analysis 1: simulated XX (top) and YY (bottom) stress magnitudes measured at the history

462 points, $K_x = K_y = 0.4$. Location of history points 1 to 5 shown in Figure 11D.

463

464   The graphs show how the X-stresses (SXX) reach positive values at history points number 2, 3 and 5 (up

465   to 0.04 MPa at the history point 2) and how they have very low negative values (compressive) at history

466   points 1 and 4. Moreover, all the history points show that Y-stresses (SYY) are very low and close to

467   positive values but that tensile stresses are not observed. It is important to note that, owing to the lack of

468   field in-situ stress measurements these results assume an initial $K_x=K_y$ value of 0.4 and do not take into

469   account probable tectonic in-situ stresses; the results consequently show relative stress changes with

470   excavation only and not the true absolute values.

471   In order to understand how the assumed in-situ stress ratio may influence the results of the study, further

472   analyses were carried using different K_x, K_y values and stress tensors. The software WinTensor 4.0.4 [23]

473   was used for this purpose.

474

475   *6.2 Stress distribution analysis based on palaeostress tensor calculation and assumed K value*

476

477   The main palaeostress tensor acting in the study area was estimated by the software WinTensor 4.0.4

478   using a stress inversion technique based on fault and joint measurements. The inversion is based on the

479   assumption that slip on a plane occurs in the direction of the maximum resolved shear stress [18]. The

480   data used for this process are the strike and dip of the fault planes, the orientation of the slip line and the

481   sense of movement on the fault planes (which can be determined from grooves or slickensides). Data is

482   inverted to obtain the characteristic parameters of the reduced palaeostress tensor according to Angelier

483   and Mechler [5] and Delvaux [24]. The derived parameters refer to the attitude of the three principal

484   stress axes σ_1, σ_2, σ_3 (where $\sigma_1 > \sigma_2 > \sigma_3$) and to the stress ratio R (Equation 5) which expresses the

485   magnitude of the intermediate principal stress, σ_2 relative to the magnitude of the major and minor

486   principal stresses σ_1 and σ_3 respectively. Some examples of the use of this software in the study of stress

487   fields in different parts of the world are given in [59], [26], [24], [25], [76].

488

489    $R = (\sigma_2 - \sigma_3) / (\sigma_1 - \sigma_3)$ with $0 < R < 1$ Equation 5

490

491   The analysis in WinTensor 4.0.4 was based on 20 measurements of kinematic indicators found on two

492   different sides of the buttress and indicated two extensional regimes ($\sigma_1 = \sigma_v$) with two different stress

493   tensors (Table 6). From the geological evidence visible in the area and in accordance with Bigazzi et al.

494   [10], Carmignani and Kligfield [17] and Ottria and Molli [61], it is suggested that these two stress tensors

495   are related to two different tectonic stages (so-called "D2S1" and "D2S2") within the D2 tectonic phase.

496   During the older stage (D2S1), strike-slip and extensional movements with a general East-West

497   orientation took place at the same time (stress tensor 1 in Table 6). During the subsequent D2S2 further

498   tectonic denudation and unloading changed the deformation style toward a multi-directional extension

499   which was probably North-South directed within the study area (stress tensor 2 in Table 6).

500

Stress Tensors	R	Type
1	0.5	Pure Extensional (nearly E-W orientation)
2	0.5	Pure Extensional (nearly N-S orientation)

501   Table 6. Stress tensors determined from analysis using WinTensor 4.0.4

502

503   Based on these results, two further FDM analyses (Analysis 2 and 3) were carried out simulating the latest

504   extensional regime (North-South directed). As the Y axis corresponds, in this case, to the North-South

505   direction, σ_y was set as the minor principal stress (σ_3) to reproduce the North-South directed extensional

506   regime. The same lithostatic vertical stress σ_v, adopted in Analysis 1, was used and the K_x and K_y values

507   were assumed as 0.6 and 0.4 respectively for Analysis 2 and 0.8 and 0.4 for Analysis 3.

508   Figures 14 and 15 show the results in terms of the simulated stress distribution in the X and Y directions

509   for Analysis 2 ($K_x = 0.6$ and $K_y = 0.4$) and Analysis 3 ($K_x = 0.8$ and $K_y = 0.4$). Figures 16 and 17 show the

510   simulated magnitude of stress values in Analysis 2 and 3 respectively at the same history points as used in

511   Analysis 1. The two simulations confirm that positive (tensile) stress values can be reached in the buttress

512   in the X direction (history points 2, 3, 4 and 5 for both Analysis 2 and 3). This agrees with field

513   observations of the presence of visible stress-induced damage in the marble buttress noted during the

514   engineering geological and photogrammetric surveys (Figure 8). Moreover, in these two analyses the

515   magnitude of the tensile stresses are greater than obtained in Analysis 1(up to 0.15 MPa for the history

516   point 2 in the analysis 2 and up to 0.2MPa for the same history point in Analysis 3).
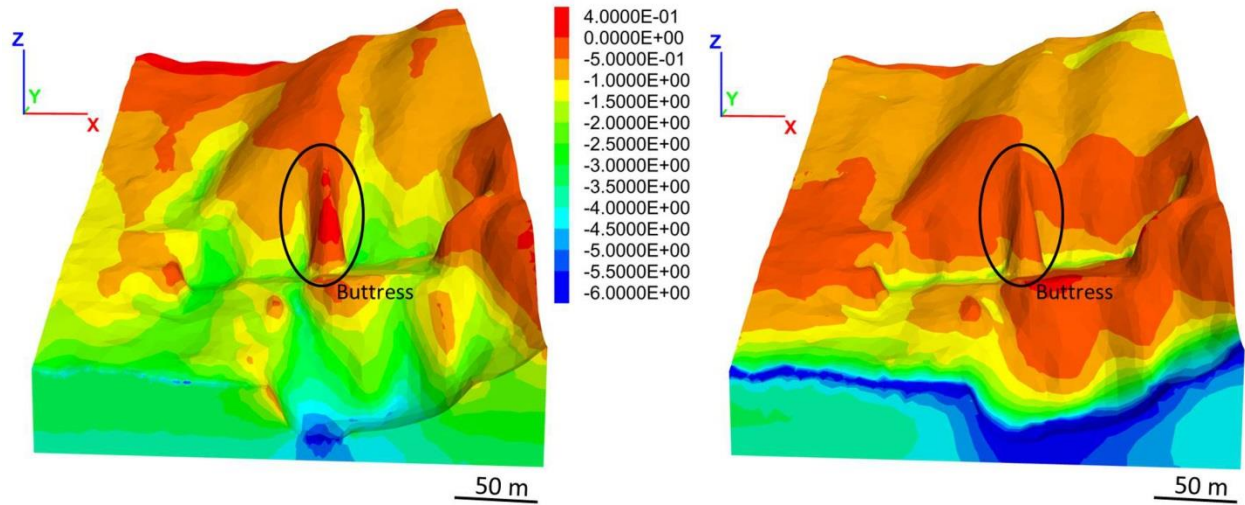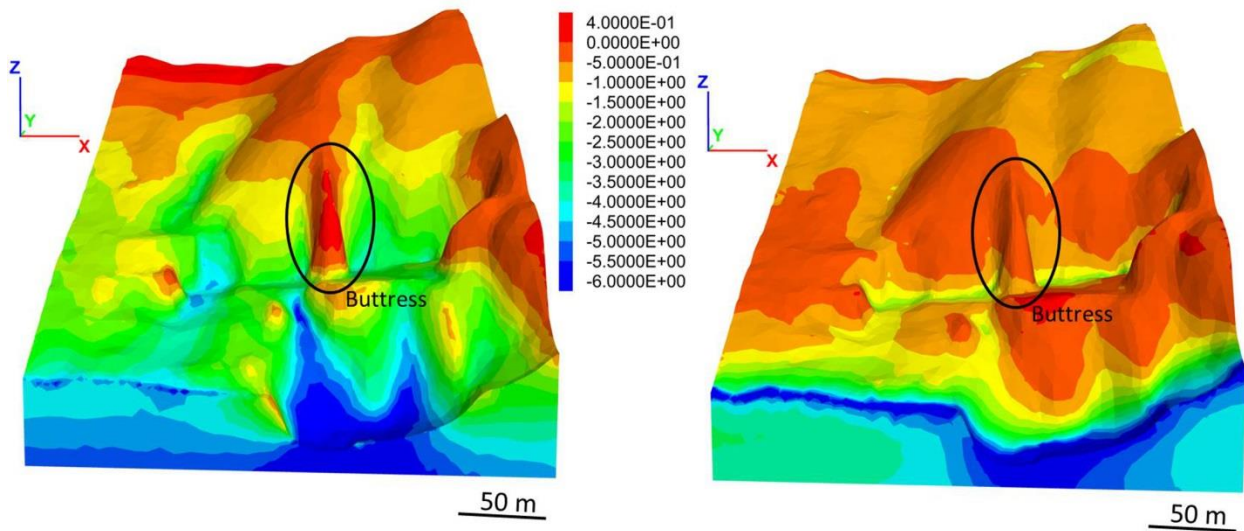
517

518

519　Figure 14: FLAC3D models for Analysis 2 showing the simulated stress distribution and magnitude; SXX

520　stress distribution in X direction (left) and SYY stress distribution in Y direction (right), $K_x = 0.6$ and K_y

521　$= 0.4$. Units of stress in MPa.

522

523

524　Figure 15: FLAC3D models for Analysis 3 showing the simulated stress distribution and magnitude; SXX

525　stress distribution in X direction (left) and SYY stress distribution in Y direction (right), $K_x = 0.8$ and K_y

526　$= 0.4$. Units of stress in MPa.

527
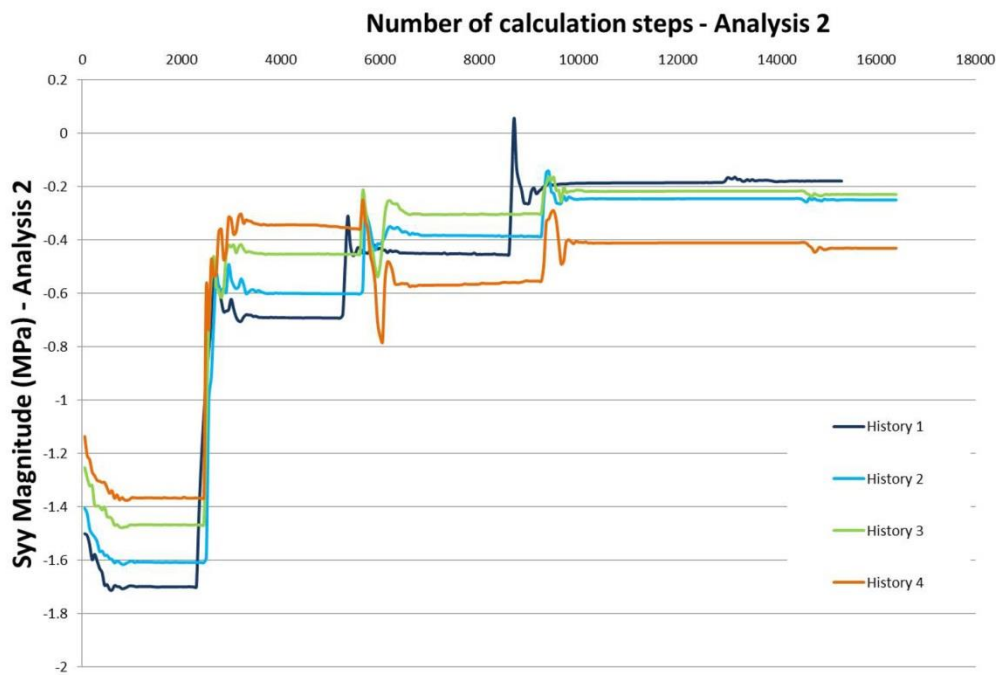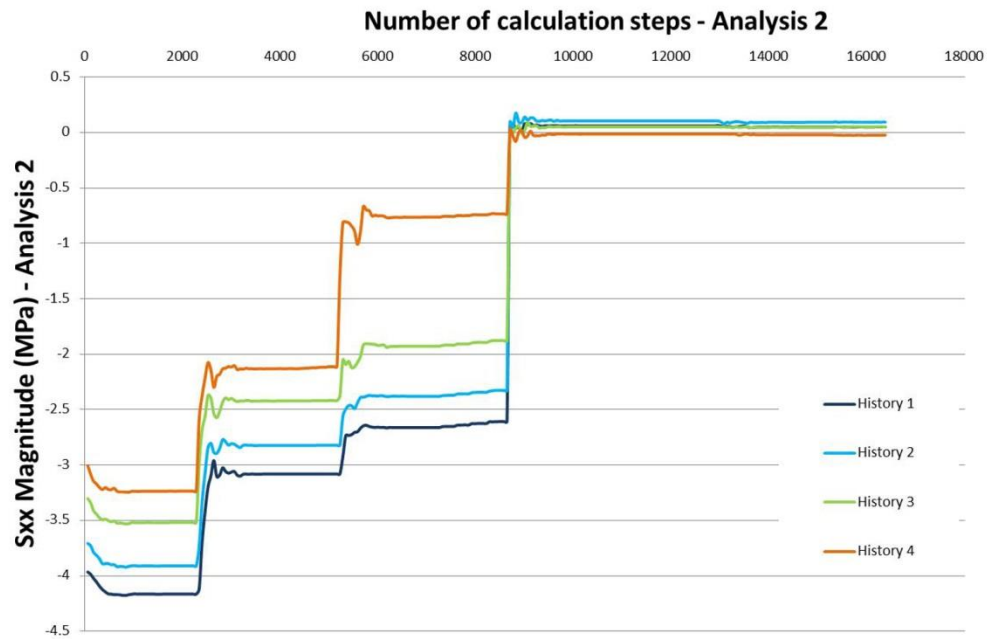
528

529 Figure 16. Analysis 2: simulated XX (top) and YY (bottom) stress magnitude measured at the history

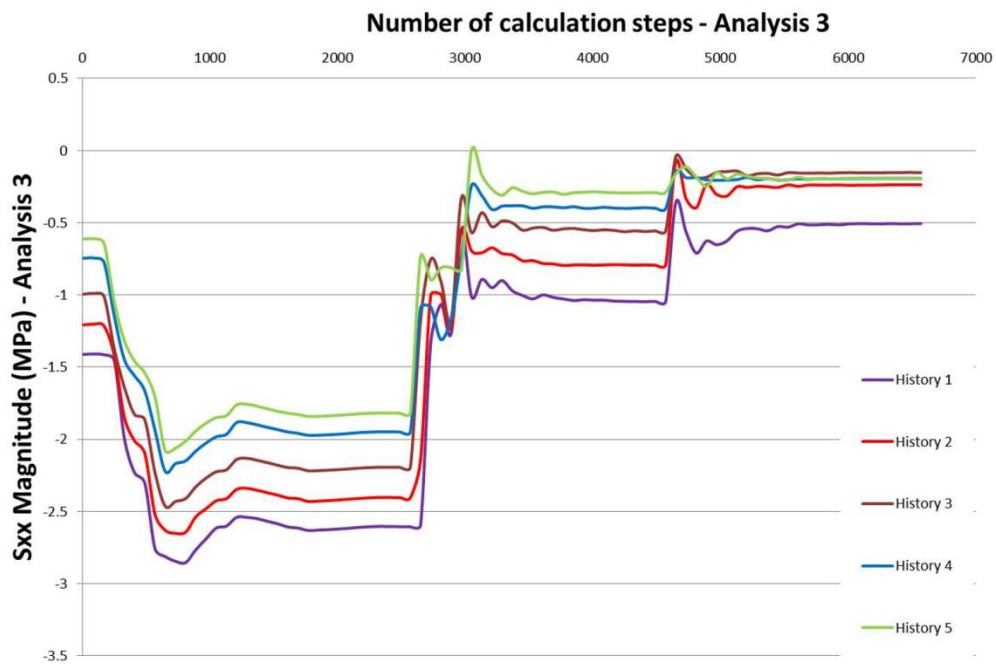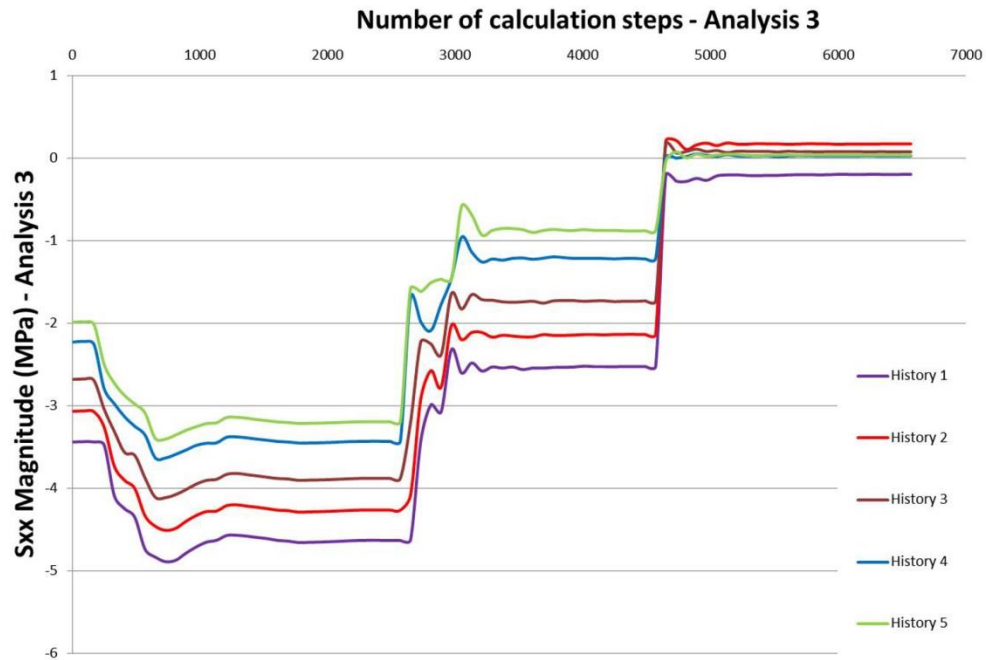530 points, $K_x = 0.6$ and $K_y = 0.4$. Location of history points 1 to 5 shown in Figure11D.

531

532   Figure 17. Analysis 3: simulated XX (top) and YY (bottom) stress magnitude measured at the history

533   points, $K_x = 0.8$ and $K_y = 0.4$. Location of history points 1 to 5 shown in Figure11D.

534

535

536

7 Discussion

This research demonstrates how an integrated remote sensing - GIS approach can improve the overall understanding and the quality of data available for rock slope stability analysis. Recently, several DTP techniques have been used by various authors to demonstrate their potential advantages in conducting surveys in high and complex geometry rock slopes. Sturzenegger and Stead (2009a and b) showed how, with the use of a tripod and long range focal length camera lenses, it is possible to calculate the joint attitude with accuracies similar to those obtained from TLS. However, in case of complex rock slope geometry and where problems of inaccessibility are encountered, this system tends to leave shadow (occluded) areas in the output. Firpo et al. [33] and Francioni et al. [34] showed how the use of an aerostatic balloon can solve problems related to the complexity of the slope, however, the inaccessibility of the area facing the object under study can be an insurmountable problem. Salvini et al. [69] and [71], clearly illustrated how the use of a helicopter can overcome the above mentioned problems. The use of helicopter systems can be both complicated and expensive and the orientation of the photographs less precise when compared to conventional terrestrial methods of survey.

In this context, the advent of UAV systems represents a very important innovation for remote sensing techniques since it provides a very powerful and flexible tool for the acquisition of high resolution photographs. Moreover, they are remotely controlled, thus avoiding the need of a crew and their cost is highly variable and dependent on the specific site requirements. The use of UAV technology in the earth sciences and more specifically in engineering geology has been documented in the literature [42], [60]. In this research the survey was executed using a vehicle that can work in an autonomous manner or be managed from the ground by remote control. Using this vehicle, it was possible to survey both the open pit surface, which is characterized by a very steep geometry, and an overhanging slope which has a complex morphology. All the photographs acquired by the UAV were oriented through the integrated use of TS and differential GPS surveys. This procedure provides a very powerful approach for increasing precision and accuracy of the photograph orientation and TLS registration procedures. The errors obtained during the exterior orientation of photographs, shown in Table 2, are considered acceptable given the survey distance and the complexity of the slope morphology. In fact, in spite of the accuracy obtained in the measurement of GCP by topographic survey, the UAV is a light and remotely controlled vehicle which can be prone to vibrations and instability phenomena during photograph acquisition. These problems can result in misalignment of photographs and significant errors during their orientation. Recently, the acquisition of a large number of photographs and the use of powerful software including image matching algorithms for the orientation process and the creation of DSM and orthophotos (see Agisoft[TM] Photoscan Professional [1]) has been shown to decrease these errors. However, if the attitude of

571   the UAV is properly controlled, the orientation of photographs permits the creation of accurate

572   stereoscopic models and the stereo-restitution and measurement of geological features such as joint

573   attitude, spacing, and trace length.

574   TLS was used in this research to obtain a very high resolution 3D model of the slope and to validate the

575   results obtained from the stereo-restitution. Three different point clouds were acquired to avoid occlusions

576   at the rock slope face and subsequently registered to a unique model thanks to the topographic survey.

577   The maximum error estimated during the registration process was approximately 5 mm which is

578   considered to be acceptable. Joint sets derived from DTP and TLS were compared (Figure 5) and show a

579   good agreement in terms of both mean dip and dip directions.

580   To complement the geomatic surveys, engineering geological surveys were carried out to provide

581   supplementary information on the physical-mechanical characteristics of the joints and the rock mass.

582   Data obtained from these surveys was used in the characterization of rock mass according to the

583   Bieniawski RMR method and for estimation of the GSI. The values of RMR and GSI made it possible to

584   classify the rock mass as "good" in accordance with previous studies [63]. It must be highlighted that the

585   engineering geological survey permitted the definition of the joint sets recognizable at the base of the

586   open pit only and, consequently it is possible to observe some differences between the values obtained

587   from DTP and TLS.

588   In addition, a kinematic analysis was carried out in order to analyse the stability of the buttress and the

589   overhanging natural slope. Considering the quality and the amount of data available from the above

590   mentioned surveys, this analysis was performed using a deterministic approach. The study area was

591   subdivided into different zones based on a spatial analysis carried out by GIS techniques. The results

592   obtained from this analysis are in agreement with previous studies carried out in the area by geologists

593   and professional hand scaling personnel and with the mitigation work previously carried on the slope

594   [63].

595   The last component of this research was a FDM analysis of the stress distribution in the buttress broadly

596   representative of its geological history and recent excavation stages. It is known from literature how

597   stress-induced damage due to excavation is a frequent problem in mining and quarrying activities and, as

598   mentioned previously, the presence of such stress-induced fractures was found in the study area. These

599   newly generated stress-induced brittle fractures may be an important consideration in the stability of an

600   area and their study could decrease the risk of failure and increase the quality of marble in future

601   extraction works. For this reason, with the aim of improving knowledge of the stress distribution in the

602   marble buttress, FDM analyses were carried out using FLAC 3D. An initial analysis (Analysis 1) was

603   performed using the induced lithostatic stress and K_x and K_y values both equal to 0.4. The simulation

604 results showed positive tensile stresses in certain positions on the buttress. Numerous researchers have

605 recently noted the role of tensile damage on rock slopes [28], [14], [15], [74] [75].

606 It is important to emphasise that the concentration of tensile stresses may be increased if high in-situ

607 tectonic stresses are present. Since in-situ measurements regarding actual tectonic in-situ stress are not

608 available, it was decided to use the WinTensor software in an attempt to investigate the most probable

609 main stress tensors in the area. The study of palaeostress carried out with the WinTensor software helps to

610 understand how structures influenced the geological history of the area (e.g. based on the Anderson's

611 classification – Anderson, [2]). It should be emphasised however the direction of palaeostress does not

612 necessarily coincide with the current stress tensor acting today. Nevertheless, recent studies carried out in

613 the Carrara marble district have confirmed that in this area there is a good correspondence between

614 palaeostress data gained with WinTensor and the stress acting today [61], [48] [41], [31].

615 The analysis described in this paper has highlighted the presence of two main stress tensors: the first East-

616 West directed and the second North-South. This result agrees with the theory that two different tectonic

617 stages (D2S1 and D2S2) took place within the D2 phase [10], [17], [61]. Two further FDM analyses was

618 then carried out (Analysis 2 and 3) simulating the most recent extensional regime (North-South directed)

619 and using K_x and K_y values equal to 0.6 and 0.4 for the Analysis 2 and to 0.8 and 0.4 for the Analysis 3

620 respectively. From the results of the FLAC3D simulation, it was possible to show how a relatively small

621 change in in situ stress ratio, K, modifies the spatial stress distribution. In fact, when comparing the

622 results of Analysis 1, 2 and 3, it is notable how in Analyses 2 and 3 the stress values measured in the X

623 direction at history points 2, 3, 5 and 5 attain positive (tensile) values and how these values increase going

624 from Analysis 1 to 3. This agrees with field observations of the presence of visible stress-induced damage

625 in the marble buttress noted during the engineering geological and photogrammetric surveys.

626 It should be emphasised that the WinTensor analysis is based on only 20 measurements due to the

627 difficulty in finding more slickenside kinematic indicators within the area (due to erosion and

628 inaccessibility). For this reason and because of the major importance that direct measurement of stress can

629 have on future slope analyses, it is clear that the described WinTensor stress study represents a first

630 preliminary stage in improving the understanding of the in-situ stress acting in the area and that further in-

631 situ measurements would be necessary to better clarify stress response and induced damage within the

632 marble buttress.

633

634 **8. Conclusions**

635

636 In this research an integrated remote sensing - GIS approach was used to improve the overall

637 understanding and the quality of data available for the analysis of the Lorano open pit. The methodology

638   described overcomes a frequent problem related to the inaccessibility of rock slopes, owing to their

639   height, which can lead to erroneous evaluations of stability. DTP and TLS are shown to provide powerful

640   modelling and analytical tools in the study of the geometry of the slope. DTP was carried out through the

641   use of a UAV system. This technique overcomes problems related to elevation, steepness and complex

642   geometry of slope; it is less expensive than other photogrammetric techniques showed in previous

643   research such as aerostatic balloons and helicopters and with a good flight plan photogrammetric

644   acquisition of areas can be obtained that would be impossible to survey with any other vehicle or

645   methodology. TLS was performed using a long range laser scanner (up to 1 Km range) with three

646   different point clouds acquired to avoid occlusions. The TLS model was overlapped with the

647   photogrammetric model to create a high resolution 3D model useful in the definition of the main

648   geological features and in the development of the 3D slope model to be used in subsequent kinematic and

649   numerical analysis.

650   Kinematic analysis was carried out using GIS techniques. Using developed thematic maps, different

651   kinematic analyses were performed according to the varying slope geometries so as to determine the

652   steepest safe angles. As a result, this approach was able to overcome the common problem of complex

653   slope geometry encountered in kinematic slope analyses.

654   Finally, a FDM analysis of the stress distribution in the buttress was performed to verify the possibility of

655   tensile stress generation after the excavation phase. A study of palaeostress was carried out with the

656   WinTensor software to understand how structures influenced the geological history of the area. Based on

657   this study, a sensitivity analysis using different K values was performed in FLAC 3D to evaluate the

658   influence of assumed in-situ stress ratio on the simulated stress distribution in the buttress. This research

659   demonstrates that unloading due to erosion and slope excavation can lead to tensile stress in the marble

660   buttress and that this will be amplified when high in-situ stress conditions are present. The FDM

661   simulation shows that, even though the tensile stresses do not reach very high magnitudes and they might

662   not be enough to generate brittle fractures in the intact rock mass (for the Kx and Ky values until now

663   investigated), they are parallel to the X direction (West-East) which is approximately the same direction

664   as the strike of the S1 foliation surfaces that characterize most of the Apuan Alps. As the S1 foliation

665   represents the direction of weakness in the rock mass, it is suggested that S1 may have an important

666   control on the nucleation and propagation of brittle fracturing. Moreover, as before mentioned, the new

667   generated fractures, was observed connecting two adjacent system discontinuities.

668   This agrees with the field observations (often the brittle fractures in the Carrara marble district follow the

669   same direction as S1) and previous studies carried out in the area [18], [52] and [17]. Although this

670   research represents a preliminary study, it forms an important step and foundation for the analysis of the

buttress and a case example of stress analysis/damage in open pit slopes using a remote sensing/FDM approach.

8.1 Future developments and works

Field measurements of in-situ stress were not available for this research. As this data becomes available (in collaboration with the *Unità Sanitaria Locale* - USL1 of Massa-Carrara), further numerical modelling will be carried out to allow the absolute stress distribution during the quarry excavation phases to be better understood (particularly in order to evaluate the buttress behaviour in case of low and very low (up to $\approx 0,1$) Kx and Ky values [32].

Laboratory testing will be performed to improve the information on the mechanical properties of the marble and to better define the role of the S1 foliation in the tensile strength of the rock. Further numerical simulation will then also be undertaken using a FDEM-DFN (Discrete fracture Network) approach (e.g. Elfen and Slope Model [65] [49]) to allow simulation of stress-induced brittle fracture generation and propagation. Based on the research presented in this paper further protection works were carried out on the natural slope overhanging the open pit and three different monitoring systems installed which have been operational since 2012 [72]. The first is a geotechnical monitoring system comprising extensometers and crack-meters, and the other two are topographic systems consisting of a terrestrial interferometer and a robotic total station. Data from these instrumentation systems will form an important constrain for future rock slope damage research and constraining existing and future stability models of the buttress area.

References

[1]   Agisoft[TM] Photoscan Professional, 2014. http://www.agisoft.ru/products/photoscan.

[2]   Anderson, E. M. 1951. The Dynamics of Faulting and Dyke Formation with Application to Britain. Oliver and Boyd, Edinburgh, ed. 2:206.

704 [3] Abellán, A., Vilaplana, J.M., Martinez, J. 2006. Application of a long-range Terrestrial Laser
705 Scanner to a detailed rock fall study at Vall de Núria (Eastern Pyrenees, Spain). Engineering Geology 88,
706 136-148.

707 [4] Alvafez, W., Cocozza T., Wezel, F.C. 1974. Fragmentation of the Alpine orogenic belt by
708 microplate dispersal. Nature 248, 309-314.

709 [5] Angelier, J., Mechler, P. 1977. Sur une methode graphique de recherche des contraintes
710 principales egalement utilisable en tectonique et en seismologie: 1a methode des diedres droits, Bull. Soc.
711 Geol. France, 7(19), 1309-1318.

712 [6] Aringoli, D. Calista, M., Gentili, B., Pambianchi, G., Sciarra, N. 2008. Geomorphological
713 features and 3Dmodelling of Montelparo mass movement (Central Italy), Engineering Geology, 99, 70-
714 84.

715 [7] Beraldin, J. A. 2004. Integration of laser scanning and close-range photogrammetry— the last
716 decade and beyond. Proceedings: XXth International Society for Photogrammetry and Remote Sensing
717 (ISPRS) Congress, Istanbul, Turkey, 972-983.

718 [8] Bieniawski, Z. 1973. Engineering classification jointed rock masses. Transactions of the South
719 African Institution of Civil Engineers, 15, 335-344.

720 [9] Bieniawski, Z. 1989. Engineering Rock Masses Classification. John Wiley and Sons Inc. New
721 York, NY, USA, 272 pp.

722 [10] Bigazzi, G., di Pisa, A.,Gattiglio, M., Meccheri, M., Norelli, P. 1988. La struttura catoclastica-
723 milonitica di Foce di Mosceta, Alpi Apuane sud orientali (M. Corchia, Gruppo delle Panie). Atti Soc Sci.
724 Nat., Mem. Ser. A., 95, 105-116.

725 [11] Board, M., Chacon, E., Varona, P., Lorig, L. 1996. Comparative analysis of toppling behaviour at
726 Chuquicamata open-pit mine, Chile. Trans. Instit. Min. Metall., 105, A11-A21.

727 [12] Bott, M.H.P. 1959. The mechanisms of oblique slip faulting. Geol. Mag. 96. 109-117.

728 [13] Brideau M.A., Pedrazzini A., Stead D., Froese C., Jaboyedoff M., van Zeyl D. 2011. Three-
729 dimensional slope stability analysis of South Peak, Crowsnest Pass, Alberta, Canada. Landslides, 8, 139-
730 158.

731 [14] Cai, M., Kaiser, P.K., Martin, C.D. 2001. Quantification of rock mass damage in underground
732 excavations from microseismic event monitoring, International Journal of Rock Mechanics and Mining
733 Sciences, 38, 1135-1145.

734 [15] Cai, M., Kaiser, P.K., Tasaka, Y., Maejima, T., Morioka, H., Minami. M. 2004. Generalized
735 crack initiation and crack damage stress thresholds of brittle rock masses near underground excavations.
736 International Journal of Rock Mechanics and Mining Sciences, 41, 833-847.

737 [16]   Cai, M., Kaiser, P.K., Morioka, H., Minami, M., Maejima, T., Tasaka, Y., Kurose, H. 2007.

738 FLAC/PFC coupled numerical simulation of AE in large-scale underground excavations. International

739 Journal of Rock Mechanics and Mining Sciences, 44, 550-564.

740 [17]   Carmignani, L., Kligfield, R, 1990. Crustal extension in the Northern Apennines: the transition

741 from compression to extension in the Alpi Apuane core complex. Tectonics, v9,1275-1303.

742 [18]   Carmignani, L.,Conti, P., Fantozzi, P.L., Mancini S., Massa G., Molli G., Vaselli L. 2007. I

743 marmi delle Alpi Apuane. Geoitalia; 21, 19-30.

744 [19]   Chang C.T., Monteiro P., Nemati K., Shyu K. 1996. Behavior of marble under compression.

745 Journal of Materials in Civil Engineering, Vol. 8, No. 3, August 1996, pp. 157-170.

746 [20]   Coggan, J.S., Wetherelt, A., Gwynn, X.P., Flynn, Z. 2007. Comparison of hand-mapping with

747 remote data capture systems for effective rock mass characterisation, 11th Congress of International

748 Society for Rock Mechanics, Lisbon 2007, 9th - 13th July 2007, Proceedings of 11th Congress of the

749 International Society for Rock Mechanics - the second half century of rock mechanics, 1, 201-205.

750 [21]   Cruden, D.M. 1989. Limit to common toppling. Can Geotech J 26:737-742

751 [22]   Danzi, M., Di Crescenzo, G., Ramondini, M., Santo, A. 2013. Use of unmanned aerial vehicles

752 (UAVs) for photogrammetric surveys in rockfall instability studies. Rendiconti Online Societa Geologica

753 Italiana, 24, 82-85

754 [23]   Dahal, R.K., Hasegawa, S., Nonomura, A., Yamanaka, M., Dhakal, S. 2008. DEM-based

755 deterministic landslide hazard analysis in the Lesser Himalaya of Nepal, Georisk 2, 161-178.

756 [24]   Delvaux, D. 1993. Quaternary stress evolution in East Africa from data of the western branch of

757 the East African rift. In: Thorweihe, Schandelmeier (Eds.), Geoscientific Research in Northern Africa,

758 Balkema, Rotterdam, pp. 315-318.

759 [25]   Delvaux, D., Barth, A. 2010. African stress pattern from formal inversion of focal mechanism

760 data. Implications for rifting dynamics. Tectonophysics 482, 105-128.

761 [26]   Delvaux, D., Kervyn, F., Macheyeki, A., Temu, E.B. 2012. Geodynamic significance of the TRM

762 segment in the East African Rift (W-Tanzania): Active tectonics and paleostress in the Ufipa plateau and

763 Rukwa basin, Journal of Structural Geology, 37, 161-180.

764 [27]   Delvaux, D. Sperner, B. 2003. Stress tensor inversion from fault kinematic indicators and focal

765 mechanism data: the TENSOR program. In: New Insights into Structural Interpretation and Modelling (D.

766 Nieuwland Ed.). Geological Society, London, Special Publications, 212: 75-100.

767 [28]   Diederichs, M.S., 1999. Instability of hard rock masses: the role of tensile damage and relaxation.

768 PhD thesis, University of Waterloo.

769 [29] Diederichs, M.S, Kaiser, P.K., Eberhardt, E. 2004. Damage initiation and propagation in hard
770 rock during tunnelling and the influence of near-face stress rotation. International Journal of Rock
771 Mechanics and Mining Sciences, 41, 785-812.

772 [30] Feng, Q.H., Röshoff, K., 2004. In-situ mapping and documentation of rock faces using a full-
773 coverage 3D laser scanner technique. International Journal of Rock Mechanics and Mining Sciences 41
774 (3), 139-144.

775 [31] Ferrero, A. M., Forlani G., Rondella R., Voyat H.I. 2009. Advanced geostructural survey methods
776 applied to rock mass characterization. Rock Mech Rock Eng 42 (4), 631-65.

777 [32] Ferrero A.M., Gullì D., Migliazza M., Segalini A. 2013. In situ stress measurements
778 interpretations in large underground marble quarry by 3D modeling. International Journal of Rock
779 Mechanics and Mining Sciences, Vol. 60, pp. 103-113.

780 [33] Firpo, G., Salvini, R., Francioni, M., Ranjith, P.G. 2011. Use of Digital Terrestrial
781 Photogrammetry in rock slope stability analysis by Distinct Element numerical methods. International
782 Journal of Rock Mechanics and Mining Science, 48 (7), 1045-1054.

783 [34] Francioni. M., Salvini, R., Stead, D. Litrico, S. 2014. A case study integrating remote sensing and
784 distinct element analysis to quarry slope stability assessment in the Monte Altissimo area, Italy.
785 Engineering Geology, 183, 290-302.

786 [35] Francioni M. 2013. Development in the study of rock slopes: an integrated remote sensing –
787 stability analysis approach. PhD thesis. University of Siena.

788 [36] Francioni, M, Girgenti C. and Vanneschi C. 2013. Underground quarrying industry and terrestrial
789 laser scanning. Proceedings to IX Convegno Giovani Ricercatori di Geologia Applicata. Napoli, Italy,
790 14th - 15th February 2013.

791 [37] Fröhlich, C., Mettenleiter, M. 2004. Terrestrial laser scanning — new perspectives in 3D
792 surveying. In: Thies, M., Koch, B., Spiecker, H., Weinacker, H. (Eds.), Laser-scanners for Forest and
793 Landscape

794 [38] Ghirotti, M., Genevois, R. 2007. A complex rock slope failure investigated by means of
795 numerical modelling based on laser scanner technique. In Proceedings: 1st Canada-US Rock Mechanics
796 Symposium, Eds E, Eberhardt, D. Stead and T. Morrison, May 27-31, Vancouver, 917-924.

797 [39] Goodman, R.E. 1989. Introduction to rock mechanics, 2nd edn. Wiley, New York, p 576

798 [40] Goodman, R.E., Bray, J.W. 1976. Toppling of rock slopes. In: Rock engineering for foundations
799 and slopes, Proceedings of a Specialty Conference vol. 2. American Society of Civil Engineering, New
800 York, p. 201-234.

801 [41]   Gullì, D., Pellegri, M., Cortopassi, A. 2010. Experimental study for stress analysis on different
802 Carrara marble underground quarries. International Symposium on Deformation Characteristics of
803 Geomaterials, September 1-3, Seoul, Korea, 1296 - 1302.

804 [42]   Haarbrink, R.B., Eisenbeiss, H. 2008. Accurate DSM production from unmanned helicopter
805 systems. International Archives of Photogrammetry, Remote Sensing and Spatial Information Sciences,
806 XXXVII/B1. PRC, Beijing, 159-164.

807 [43]   Handley, M. F., Karparov, K. N. 2007. Proposed thrust failure analytical method for slope
808 collapse in open pit mines," in The Second Half Century of Rock Mechanics (11th Congress of the
809 International Society for Rock Mechanics, Lisbon, July 2007), Vol. 1, pp. 645-652, L. Ribeiro e Sousa, C.
810 Olalla, and N. Grossmann, Eds. London: Taylor & Francis Group.

811 [44]   Haneberg, W.C. 2008. Using close range terrestrial digital photogrammetry for 3-D rock slope
812 modelling and discontinuity mapping in the United States. Bulletin of Engineering Geology and the
813 Environment, 67: 457-469.

814 [45]   Hoek, E., Brown, E.T. 1997. Practical estimates of rock mass strength. International Journal of
815 Rock Mechanics and Mining Sciences 34 (8), 1165-1186.

816 [46]   Hoek, E., Bray, J.W. 1981. Rock slope engineering, Third edition. The Institution of Mining and
817 Metallurgy, London, 358 pp.

818 [47]   Hoek, E., Diederichs, M.S. 2006. Empirical estimation of rock mass modulus. International
819 Journal of Rock Mechanics and Mining Sciences 43 (2), 203-215.

820 [48]   Iabichino, G., Gullì, D., Cravero M., Bianchini, S. 2006. Comparison between 2D overcoring and
821 hydraulic fracturing stress measurements in the Apuane Alps. In-situ Rock Stress – Lu, Li, Kjørholt &
822 Dahle (eds) Taylor & Francis Group, London, ISBN 0-415-40163-1

823 [49]   Itasca Software 2012. FLAC3D; Kubrix; Slope Model. http://www.itascacg.com/software/flac3d

824 [50]   Jaboyedoff M, Baillifard F, Couture R, Locat J, Locat P. 2004. Toward preliminary hazard
825 assessment using DEM topographic analysis and simple mechanic modeling. In: Lacerda WA, Ehrlich M,
826 Fontoura AB, Sayo A (eds) Proceedings of the 9th International symposium on landslides. Balkema,
827 Rotterdam, pp 191-197

828 [51]   Jaboyedoff, M., Oppikofer, T., Minoia, R., Locat, J., Turmel, D. 2008. Terrestrial LIDAR
829 investigation of the 2004 rockslide along Petit Champlain Street, Québec City (Québec, Canada).
830 Proceedings: 4th Canadian Conference on Geohazards, 20-24May, Québec, Canada, 8 pp.

831 [52]   Kligfield, R. 1979. The Northern Apennines as a collisional orogeny. Am. J. Sci. 279, 676-69.

832 [53]   Kraus, K. 2007. Photogrammetry, Geometry from Images and Laser Scans. Berlin: De Gruyter.

833 [54] Lato, M., Diederichs, M.S., Hutchinson, D.J., Harrap, R. 2009. Optimization of LiDAR scanning

834 and processing for automated structural evaluation of discontinuities in rock masses. International Journal

835 of Rock Mechanics and Mining Sciences 46, 194-199.

836 [55] Lightfoot, N., Maccelari, M.J. 1999. Numerical Modelling of Mine Workings. SIMRAC Final

837 Project Report GAP 415. Pretoria: Department of Minerals and Energy.

838 [56] Linder, W., 2003. Digital Photogrammetry - Theory and Applications. Heidelberg.

839 [57] Marinos, V., Marinos, P., Hoek E, 2005. The geological strength index: applications and

840 limitations. Bull Eng Geol Environ 64:55-65.

841 [58] Maurenbrecher P.M., Hack H.R.G.K. 2007. Toppling mechanism: resolving the question of

842 alignment of slope and discontinuities. In: Ribeiro e Sousa L, Ollala C, Grossmann N, (eds) 11th

843 Congress of the International Society for Rock Mechanics. Taylor and Francis, London, pp 725-728.

844 [59] McNeel and Associates, 2011. Rhinoceros 4, SR9. http://www.rhino3d.com/download/rhino/4.0.

845 [60] Niethammer, U., Rothmund S., James M. R., Travelletti J., Joswig M. 2010. UAV-based remote

846 sensing of landslides. International Archives of Photogrammetry, Remote Sensing and Spatial

847 Information Sciences, Vol. XXXVIII, 496 - 501.

848 [61] Ottria G., Molli G. 2000. Superimposed brittle structures in the late-orogenic extension of the

849 northern Apennine: results from the Carrara area (Alpi Apuane, NW Tuscany). Terra Nova, Vol. 12, 52-

850 59.

851 [62] Perazzelli P., Graziani A., Rotonda T. 2009. Stability analysis of an active marble quarry by

852 DEM modelling. Proceedings of the International Conference on Rock Joints and Jointed Rock Masses,

853 Arizona, USA, January 7-8, 2009.

854 [63] Profeti, M., Cella, R. 2010. Relazione sulla stabilità dei fronti – Cava Lorano n. 22. Technical

855 report.

856 [64] Richards, L.R., Leg, G.M.M., Whittle, R.A. 1978. Appraisal of stability conditions in rock slopes.

857 In: Bell FG (ed) Foundation engineering in difficult ground. Newnes-Butterworths, London, pp 449-512.

858 [65] Rockfield 2012. ELFEN 2D/3D Numerical Modelling Package. Rockfield Software Ltd.,

859 Swansea. http://www.rockfield.co.uk/

860 [66] Rocscience 2014. Rocscience software products - DIPS 6.0, RocData 5.0.

861 https://www.rocscience.com.

862 [67] Roncella, R., Forlani, G., Remondino, F. 2005. Photogrammetry for geological applications:

863 automatic retrieval of discontinuity orientation in rock slopes. In: Proc SPIE-IS&T electronic imaging,

864 Videometrics 5665,17-27.

865 [68] Sainsbury, B., Pierce, M. Mas Ivars, D. 2008. Analysis of Caving Behavior Using a Synthetic

866 Rock Mass - Ubiquitous Joint Rock Mass Modeling Technique, In Proceedings of the 1st Southern

Hemisphere International Rock Mechanics Symposium (SHIRMS), Y. Potvin, J. Carter, A. Dyskin and R. Jeffrey (eds), 16 - 19 September 2009, Perth, Australia, Australian Centre for Geo-mechanics, Perth, Vol. 1 - Mining and Civil, pp. 243 - 254.

[69] Salvini, R., Francioni, M., Fantozzi, P.L., Riccucci, S., Bonciani, F., Mancini, S. 2011. Stability analysis of "Grotta delle Felci" Cliff (Capri Island, Italy): structural, engineering-geological, photogrammetric surveys and laser scanning. Bull. Eng Geol Environ 70, 549-557.

[70] Salvini, R., Francioni, M. 2013. Geomatic for slope stability and rock fall runout analysis: a case study along the Alta Tambura road in the Apuan Alps (Tuscany, Italy). Italian Journal of Engineering Geology and Environment. Book series 6, Genevois R and Prestininzi A. (eds.), 481-492.

[71] Salvini, R., Francioni, M., Riccucci, S., Bonciani, F., Callegari, I. 2013. Photogrammetry and laser scanning for analyzing slope stability and rock fall runout along the Domodossola–Iselle railway, the Italian Alps. Geomorphology 185, 110-122.

[72] Salvini R., Vanneschi C., Gullì D., Forchione F., Riccucci S. and Francioni M. 2014. Integration of geotechnical and remote monitoring systems for the analysis and control of ground deformation in marble quarrying (Apuan Alps, Italy). in "Engineering Geology for Society and Territory. Vol. 5 Urban Geology, Sustainable Planning and Landscape Exploitation", Lollino G., Manconi A., Guzzetti F., Culshaw M., Bobrowsky P. and Luino F. (eds.), 183-188.

[73] Slama, C.C. (Ed.) 1980. Manual of Photogrammetry, 4th edition. American Society of photogrammetry, Falls Church, 1056 pp.

[74] Stead, D., Eberhardt, E., Coggan, J.S. 2004. Modelling of complex rock slope failure mechanisms using a hybrid finite-/discrete-element code. 1067-1072. in Landslides Evaluation and Stabilization. ISBN 04 1535 667 9 Proc IXth ISL, Eds Lacerda et al. Rio de Janeiro, 2004.

[75] Stead, D., Eberhardt, E. 2013. Understanding the mechanisms of large landslide. Vaiont 2013, Italian Journal of Engineering Geology, Italian journal of engineering geology and environment. Book series 6, Genevois R. and Prestininzi A. (eds.), 85 - 112

[76] Sturzenegger, M., Stead, D., Beveridge, A., Lee, S., van As., A. 2009. Long-range terrestrial digital photogrammetry for discontinuity characterization at Palabora open-pit mine. In Diederichs M. & Grasselli G. eds. "ROCKENG09: Proceedings of the 3rd CANUS Rock Mechanics Symposium", Toronto, paper 3984, 10 pp.

[77] Sturzenegger, M., Stead, D. 2009(a). Close-range terrestrial digital photogrammetry and terrestrial laser scanning for discontinuity characterization on rock cuts. Engineering Geology 106, 163-182.

899   [78]   Sturzenegger, M., Stead, D. 2009(b). Quantifying discontinuity orientation and persistence on

900   high mountain rock slopes and large landslides using terrestrial remote sensing techniques. Natural

901   Hazards and Earth System Sciences 9 (2), 267-287.

902   [79]   Tonon, F., Kottenstette, J.T. 2007. Laser and photogrammetric methods for rock face

903   characterization. Report on a Workshop Held in Golden, Colorado, June 17-18, 2006. American Rock

904   Mechanics Association, 6 pp.

905   [80]   Vandeginste, V., Faure, J.L., Osadetz, K., Roure, F. Swennen, R. 2012. Paleostress evolution in

906   the Canadian Cordilleran foreland fold-and-thrust belt west of Calgary. Geologica Belgica, Vol. 15/1-2,

907   pp. 42-52.

908   [81]   Van Westen, C.J. 1998. GIS in landslide hazard zonation: a view, with cases from the Andes of

909   Colombia, in: F.P. Martin, D.I. Heywood (Eds.), Mountain Environment and Geographic Information

910   Systems, Taylor & Francis, pp. 35-165.

911   [82]   VanWesten, C.J., Terlien, M.T.J. 1996. Deterministic landslide hazard analysis in GIS: a case

912   study from Manizales (Colombia), Earth Surface Processes and Landforms, 21, 853-868.

913   [83]   Wiles, t. d. 2005. Reliability of numerical modelling predictions. International Journal of Rock

914   Mechanics and Mining Sciences, Vol. 43, 454-472

915   [84]   Xie, M., Esaki, T., Cai M.F. 2004. A GIS-based method for locating the critical 3D slip surface in

916   a slope, Computers and Geotechnics, 31, 267-277.

917   [85]   Xie, M., Esaki, T., Qiu, C., Wang C.X. 2006. Geographical information system-based

918   computational implementation and application of spatial three-dimensional slope stability analysis,

919   Computers and Geotechnics, 33, 260-274.

920

921

922